

Analysis of Heme Iron Coordination in DGCR8: The Heme-Binding Component of the Microprocessor Complex

Hazel M Girvan, Justin M. Bradley, Myles R. Cheesman, James R. Kincaid, Yilin Liu, Kazimierz Czarnecki, Karl Fisher, David Leys, Stephen E. J. Rigby, and Andrew William Munro

Biochemistry, **Just Accepted Manuscript** • DOI: 10.1021/acs.biochem.6b00204 • Publication Date (Web): 20 Aug 2016

Downloaded from <http://pubs.acs.org> on August 24, 2016

Just Accepted

“Just Accepted” manuscripts have been peer-reviewed and accepted for publication. They are posted online prior to technical editing, formatting for publication and author proofing. The American Chemical Society provides “Just Accepted” as a free service to the research community to expedite the dissemination of scientific material as soon as possible after acceptance. “Just Accepted” manuscripts appear in full in PDF format accompanied by an HTML abstract. “Just Accepted” manuscripts have been fully peer reviewed, but should not be considered the official version of record. They are accessible to all readers and citable by the Digital Object Identifier (DOI®). “Just Accepted” is an optional service offered to authors. Therefore, the “Just Accepted” Web site may not include all articles that will be published in the journal. After a manuscript is technically edited and formatted, it will be removed from the “Just Accepted” Web site and published as an ASAP article. Note that technical editing may introduce minor changes to the manuscript text and/or graphics which could affect content, and all legal disclaimers and ethical guidelines that apply to the journal pertain. ACS cannot be held responsible for errors or consequences arising from the use of information contained in these “Just Accepted” manuscripts.



1
2
3
4
5
6
7
8
9
10
11
12
13
14
15
16
17
18
19
20
21
22
23
24
25
26
27
28
29
30
31
32
33
34
35
36
37
38
39
40
41

Analysis of Heme Iron Coordination in DGCR8: The Heme-Binding Component of the Microprocessor Complex

42
43
44
45
46
47
48
49
50
51
52
53
54
55
56
57
58
59
60

*Hazel M. Girvan,[†] Justin M. Bradley,[‡] Myles R. Cheesman,[‡] James R. Kincaid,[§] Yilin Liu,[§]
Kazimierz Czarnecki,[§] Karl Fisher,[†] David Leys, Stephen E. J. Rigby,[†] and Andrew W. Munro^{*,†}*

[†]Centre for Synthetic Biology of Fine and Specialty Chemicals (SYNBIOCHEM), Manchester
Institute of Biotechnology, Faculty of Life Sciences, University of Manchester, 131 Princess
Street, Manchester M1 7DN, UK. [‡]School of Chemistry, University of East Anglia, Norwich
Research Park, Norwich NR4 7TJ, UK. [§]Department of Chemistry, Marquette University, 535
North 14th Street, Milwaukee WI 53233, USA.

Keywords. DGCR8, Heme iron coordination, EPR, Magnetic Circular Dichroism, resonance
Raman spectroscopy.

Corresponding Author. *Professor Andrew W. Munro, Centre for Synthetic Biology of Fine
and Specialty Chemicals (SYNBIOCHEM), Manchester Institute of Biotechnology, Faculty of
Life Sciences, University of Manchester, 131 Princess Street, Manchester M1 7DN, UK. Phone:
0044-161-306-5151. E-mail: Andrew.Munro@Manchester.ac.uk.

1
2
3 **Abbreviations.** DGCR8, DiGeorge critical region 8 protein; ENDOR, electron-nuclear double
4 resonance spectroscopy; EPR, electron paramagnetic resonance spectroscopy; MCD, magnetic
5 circular dichroism spectroscopy; miRISC, miRNA induced silencing complex; miRNA,
6 microRNA; NIR, near-infrared; pre-miRNA, precursor miRNA; pri-miRNA, primary miRNA;
7 UTR, untranslated region; UV-vis, UV-visible.

8
9
10
11
12
13
14
15
16
17
18
19
20 **ABSTRACT:** DGCR8 is the RNA binding partner of the nuclease Drosha. Their complex (the
21 “Microprocessor”) is essential for processing of long, primary microRNAs (pri-miRNAs) in the
22 nucleus. Heme binding to DGCR8 is essential for pri-miRNA processing. Based on the split
23 Soret UV-visible (UV-vis) spectrum of ferric DGCR8, *bis*-thiolate sulfur (cysteinate, Cys⁻) heme
24 iron coordination of DGCR8 heme iron was proposed. We have characterized DGCR8 heme
25 ligation using the $\Delta 276$ DGCR8 variant and combined electron paramagnetic resonance (EPR),
26 magnetic circular dichroism (MCD), electron nuclear double resonance, resonance Raman and
27 electronic absorption spectroscopy. These studies indicate DGCR8 *bis*-Cys heme iron ligation,
28 with conversion from *bis*-thiolate (Cys⁻/Cys⁻) axial coordination in ferric DGCR8 to *bis*-thiol
29 (CysH/CysH) coordination in ferrous DGCR8. Pri-miRNA binding does not perturb ferric
30 DGCR8’s optical spectrum, consistent with the axial ligand environment being separated from
31 the substrate binding site. UV-vis absorption spectra for the Fe^{II} and Fe^{II}-CO forms indicate
32 discrete species exhibiting peaks with absorption coefficients substantially larger than those for
33 ferric DGCR8, and for that previously reported for a ferrous form of DGCR8. ENDOR data
34 exclude histidine or water as axial ligands for ferric DGCR8, and favor *bis*-thiolate coordination
35 in this form. UV-vis MCD and near-infrared MCD provide data consistent with this conclusion.

1
2
3 UV-vis MCD data for ferrous DGCR8 reveal features consistent with *bis*-thiol heme iron
4
5 coordination, and resonance Raman data for the ferrous-CO form are consistent with a thiol
6
7 ligand *trans* to the CO. These studies support retention of DGCR8 cysteine coordination upon
8
9 reduction, a conclusion distinct from previous studies on a different ferrous DGCR8 isoform.
10
11
12
13
14
15
16

17
18 MicroRNAs (miRNAs) are a large family of short (~22 nucleotide) noncoding RNAs with
19
20 fundamental roles in the regulation of cellular function in animals and plants, and in certain
21
22 viruses. Most animal miRNAs base pair (imperfectly) to sequence regions in the 3'-untranslated
23
24 region (UTR) of their target mRNAs (1). In so doing, they cause inhibition of protein synthesis
25
26 by either repressing translation, or by promoting the deadenylation and degradation of the
27
28 mRNA (2-5). The crucial importance of miRNAs in gene regulation is now well understood, and
29
30 it is thought that miRNAs control the activity of over half of all mammalian protein-coding
31
32 genes (1).
33
34
35
36
37

38 In the canonical route for their production, miRNAs are synthesized in a multi-stage
39
40 pathway which begins in the nucleus with transcription of long (often kb) primary miRNA (pri-
41
42 miRNA) species by RNA polymerase II, usually with both a 5' cap and a poly-A tail (6, 7). Pri-
43
44 miRNA has a ~80 base hairpin, flanked at both the 3' and 5' ends by single stranded RNA (8).
45
46 These pri-miRNA transcripts are cleaved into shorter (~65 nucleotide) precursor miRNA (pre-
47
48 miRNA) hairpins (9, 10), by the RNase III enzyme Droscha (11). Droscha is incapable of pri-
49
50 miRNA cleavage in isolation, instead working as part of the Microprocessor complex with
51
52 DGCR8 (DiGeorge critical region 8 protein) (12-15). Droscha contains two RNase III domains
53
54 (RIIIda and RIIIdb) which cleave the 3' strand and 5' strand of the pre-miRNA, respectively,
55
56
57
58
59
60

1
2
3 leaving an overhang on the 3' protruding end for recognition by Exportin 5 (10, 11). Following
4
5 nuclear export by Exportin 5, the pre-miRNA is further cleaved by the RNase III enzyme Dicer,
6
7 forming a 22 nucleotide miRNA:miRNA* duplex (16-18). One strand of the duplex remains as
8
9 the mature miRNA, becoming incorporated into the miRISC (miRNA induced silencing
10
11 complex) (19, 20), where the miRNA base pairs to target mRNA, usually in the 5' UTR (5'
12
13 untranslated region), inducing either translational repression or mRNA degradation (2-5). The
14
15 other strand (the "passenger" miRNA, or miRNA*) is typically released and degraded, but can
16
17 also be incorporated into the miRISC complex and function as a *bona fide* miRNA (21-23).
18
19 Alternative routes for miRNA biogenesis which do not rely on one or both of the Microprocessor
20
21 or Dicer systems have been discovered (24). For example, in the mirtron pathway short hairpins
22
23 are generated with splice acceptor and donor sites, and a splicing event replaces the Drosha
24
25 cleavage step before the pathway continues as described above. Alternatively, miRNA synthesis
26
27 can occur in a Microprocessor-dependent, Dicer-independent manner in which pre-miRNA is
28
29 loaded into Argonaute (a catalytic component of the miRISC complex), and where a number of
30
31 further cleavage steps ultimately result in miRNA formation (1, 24).
32
33
34
35
36
37
38
39

40 The processing of long pri-miRNA transcripts into shorter pre-miRNAs by the
41
42 Microprocessor complex is a key step in the canonical pathway of miRNA generation. The
43
44 Drosha RNase III is crucial for nuclear miRNA processing, and is a key component of the
45
46 Microprocessor (11). However, it is incapable of miRNA cleavage without its DGCR8 partner
47
48 (12-15). DGCR8 is a 773 amino acid protein that contains two dsRNA binding domains at the C-
49
50 terminus (25) and a WW motif (13), and also binds a heme prosthetic group (26). DGCR8 can be
51
52 truncated into an active form named NC1 (amino acids 276-751) which contains both the heme-
53
54 binding domain (HBD, amino acids 276-498) and two double-stranded RNA binding domains
55
56
57
58
59
60

1
2
3 (amino acids 499-751) followed by a short tail region (10). A dimerization domain was also
4 identified within the independently folded HBD (amino acids 276-353) and its crystal structure
5 was solved in a dimeric state. These data revealed a key role for the WW motif region in
6 formation of the domain-swapped dimer and implicated this region in association with the heme
7 cofactor in DGCR8 (27). The dsRNA binding domains of DGCR8 form the binding site for pri-
8 miRNA (8), and the C-terminal region is responsible for Drosha's interactions with DGCR8
9 (28). DGCR8 and Drosha are the minimum requirement for the processing of pri-miRNA to pre-
10 miRNA (13, 15). However, other proteins, including p53 and nucleolin, bind to the
11 Microprocessor complex to influence its activity, either by increasing or decreasing the rate of
12 processing of a subset of miRNAs (29, 30). Heme-bound DGCR8 is essential for catalytic
13 function of the Microprocessor complex (31). Quick-Cleveland *et al.* showed that the HBD is
14 crucial for the binding and recognition of pri-miRNA by DGCR8, and that heme is essential to
15 produce processing-competent DGCR8/pri-miRNA complexes (32).
16
17
18
19
20
21
22
23
24
25
26
27
28
29
30
31
32
33
34

35 Early studies proposed that axial coordination of the DGCR8 heme *b* came from a
36 cysteine residue (26), potentially making DGCR8 a member of the growing class of heme
37 thiolate proteins. Other notable heme thiolate proteins are the widely studied cytochrome P450
38 (P450 or CYP) monooxygenases, and the nitric oxide synthases which catalyze oxidative
39 transformation of *L*-arginine to *L*-citrulline and nitric oxide (33). Numerous examples of heme
40 thiolate proteins have been discovered with diverse functions. These include the heme sensors
41 Rev-erba and Rev-erbβ, which are nuclear receptors and transcriptional repressors, and which
42 bind heme to enable interaction with co-repressor proteins and to regulate transcription in
43 circadian rhythm pathways (34). Another example is the CO sensing transcription factor CoxA
44 from *Rhodospirillum rubrum*, a bacterium which uses CO as a carbon source under anaerobic
45
46
47
48
49
50
51
52
53
54
55
56
57
58
59
60

1
2
3 conditions. CooA uses a ligand switching mechanism whereby a cysteine ligand to the heme iron
4
5 is displaced by a histidine when the heme iron is reduced. In the dimeric CooA structure, the
6
7 other axial ligand comes from the N-terminal proline of the opposite monomer. This proline is
8
9 displaced by CO, and the structural change induced enables the exposure of DNA-binding
10
11 domains in CooA. The transcriptionally competent CooA can then activate the expression of
12
13 genes required for oxidation of CO to CO₂ and for the reduction of protons to H₂ (34, 35).
14
15
16
17

18
19 Previous studies on DGCR8 reported that Cys352 is involved in heme binding, although
20
21 the identity of the axial ligand *trans* to the cysteine was not identified (26). Barr *et al.* then
22
23 reported spectroscopic data consistent with *bis*-cysteine ligation of the heme iron, and suggested
24
25 that a single heme was coordinated by Cys352 side chains from both DGCR8 proteins in a
26
27 dimer. The ferric heme form was later identified as crucial for pri-miRNA processing, with the
28
29 ferrous heme form being inactive and exhibiting an increased heme dissociation rate from the
30
31 protein. In the previous study, the axial coordination state of the frog DGCR8-bound ferrous
32
33 heme was not clearly established, but it was inferred that cysteine ligation was lost and that the
34
35 ferrous heme might exist in heterogeneous spin- and coordination-states (36). In this study, we
36
37 report a detailed analysis of the heme binding site of DGCR8 using a range of spectroscopic
38
39 techniques. The results allow us to assign the active ferric heme form of the human DGCR8
40
41 protein as the first *bis*-Cys ligated protein and to provide data supporting the retention of cysteine
42
43 coordination of the heme iron in the ferrous form of this physiologically important enzyme.
44
45
46
47
48
49
50
51
52
53
54
55
56
57
58
59
60

EXPERIMENTAL PROCEDURES

DCGR8 cloning, overexpression and purification. The DGCR8 gene was obtained as Addgene plasmid 10921 from the Tuschl group (15). A 276 N-terminal amino acid truncation was generated by PCR, with mutagenic oligonucleotides creating an NdeI restriction enzyme site at the new start codon and a downstream BglII site in the 3' oligonucleotide (forward primer 5'-ggcggagacagcgaccatcatatggatggagagacaagtg-3', reverse primer 5'-ctagatatctcgagatctgccgctcacacgtccacgggtgcacag-3', NdeI and BglII sites are underlined in the forward and reverse primer, respectively). The PCR product was then cloned into pET15b, which provides a 6-His N-terminal tag to the truncated DGCR8, and the correct DNA sequence was verified by complete sequencing of the cloned gene (Source BioScience, Rochdale UK).

The Δ 276 DGCR8 (the 276 N-terminal amino acid truncated form of DGCR8) was expressed in *E. coli* BL21 (DE3) cells. Transformant cell cultures were grown with shaking at 37°C until an OD₆₀₀ of 0.8 was reached. Incubation temperature was then decreased to 18°C and DGCR8 gene expression induced by addition of 0.25 mM IPTG, along with δ -aminolevulinic acid (0.2 mM) to promote heme synthesis and incorporation. Cultures were harvested by centrifugation following a further 18 hours of cell growth post IPTG induction. Bacterial cells were resuspended in 50 mM Tris (pH 8.0), 200 mM KCl buffer at 4°C (binding buffer). The cells were lysed by sonication using a Bandelin Sonopuls sonicator (10 passes at 40% full power) and DGCR8 purified by affinity chromatography, using nickel-NTA resin (Generon, Maidenhead UK) as a first step. The protein was bound to the column, washed in binding buffer, and then eluted with binding buffer plus 100 mM imidazole. The protein was exchanged into binding buffer and loaded onto a heparin Sepharose 6 Fast Flow column (GE Healthcare, Little Chalfont UK), prior to elution with binding buffer plus 500 mM KCl. Pure DGCR8 protein was obtained

1
2
3 using a final gel filtration step on a 16/600 S200 gel filtration column (GE Healthcare), with the
4 same binding buffer. Purity was assessed by SDS-PAGE using a Mini-PROTEAN TGX Stain-
5 Free 10% gel system (Bio-Rad, Hemel Hempstead UK) and by UV-vis spectroscopic
6 comparison between total protein absorbance (A_{280}) and the specific DGCR8 heme absorbance
7 (A_{450}).
8
9
10
11
12
13
14
15
16
17
18
19

20 **Preparation of RNA.** 63 nucleotide pre-miR30a and 151 nucleotide pri-miR30a complementary
21 DNAs were synthesized (Eurofins, Ebersberg, Germany) based on sequences detailed in the
22 miRBase database (37), and as described by Lee *et al.* (11) for pre- and pri-miR30a, respectively.
23
24 DNA was cloned into a plasmid containing a 3' hepatitis delta virus (HDV) ribozyme for the
25 generation of transcripts without heterogeneous 3'-ends (38). Plasmids were linearized with
26 XbaI, the site for which is downstream of the HDV ribozyme, and *in vitro* transcription was
27 carried out by the method of Gurevich (39). Transcripts were dialyzed to remove salt and free
28 nucleotides, re-concentrated by ultrafiltration using a 30,000 MWCO Vivaspin, (Sartorius,
29 Goettingen, Germany) and purified from the HDV ribozyme by electrophoresis on a 12%
30 acrylamide, 50% urea gel. The relevant RNA band was visualized by RNA shadowing, excised
31 from the gel and then purified by the crush and soak method (40).
32
33
34
35
36
37
38
39
40
41
42
43
44
45
46
47
48
49

50 **UV-vis spectroscopy.** All UV-vis spectral measurements were made on a Cary 50 Bio
51 spectrophotometer (Varian, UK) with a 1 cm pathlength cuvette. Unless otherwise stated, all
52 spectra were collected in 50 mM Tris (pH 8.0), 500 mM KCl containing 10% glycerol and at
53 20°C. The DGCR8 heme content was quantified using a coefficient of $\epsilon_{450} = 70 \text{ mM}^{-1} \text{ cm}^{-1}$ for
54
55
56
57
58
59
60

1
2
3 the oxidized (ferric) hemoprotein. This value was calculated using the pyridine hemochromagen
4 method (41).
5
6
7
8
9

10
11
12 ***Magnetic Circular Dichroism (MCD) spectroscopy.*** MCD spectra were recorded using JASCO
13 J/810 and J/730 spectropolarimeters in the UV-vis and near-IR (NIR) regions, respectively at
14 20°C. A magnetic field of 6 Tesla was generated using an Oxford Instruments superconducting
15 solenoid with a 25 mm ambient bore. A 0.1 cm pathlength quartz cuvette was used to record
16 near-IR spectra with a 70 μ M DGCR8 sample in 50 mM Tris (pH 8.0), 500 mM KCl, 10%
17 glycerol. UV-vis spectra were also recorded for a 70 μ M sample, but here using buffer prepared
18 in deuterium oxide (otherwise as above) and following extensive dialysis of the sample into the
19 deuterated buffer. A reduced DGCR8 sample was prepared by adding sodium dithionite to a 185
20 μ M sample of DGCR8 in an anaerobic glovebox environment. After allowing 4 hours incubation
21 at 20°C to ensure extensive reduction of the DGCR8 heme iron, electronic absorption and MCD
22 spectra were collected in the UV-vis region. Minor spectral contributions from residual amounts
23 of ferric DGCR8 (~15%) were accounted for by determining the proportion of ferric DGCR8
24 (with reference to the oxidized DGCR8 spectrum) and by subtracting this component from the
25 obtained ferrous DGCR8 spectrum.
26
27
28
29
30
31
32
33
34
35
36
37
38
39
40
41
42
43
44
45
46
47
48
49

50 ***Electron paramagnetic resonance (EPR) and Electron-nuclear double resonance (ENDOR)***
51 ***spectroscopic analysis of DGCR8.*** Spectra were obtained at 10 K and X-band (~ 9.5 GHz) using
52 a Bruker ELEXSYS E500/E580 spectrometer equipped with a Bruker ER 4123SHQE resonator
53 together with an Oxford instruments ESR900 cryostat for EPR measurements, and a Bruker EN
54
55
56
57
58
59
60

1
2
3 4118X-MD-4 resonator together with an Oxford instruments CF935 cryostat for ENDOR
4
5 measurements. DGCR8 spectra were collected for a 225 μM sample in 50 mM Tris (pH 8.0), 500
6
7 mM KCl, 10% glycerol. A sample was also exchanged into deuterated buffer of the same
8
9 composition by extensive dialysis, and an ENDOR spectrum was then collected at the same
10
11 protein concentration as for the non-deuterated sample. EPR experiments were done using 1 mW
12
13 microwave power and 5 G modulation amplitude at a modulation frequency of 100 KHz. The
14
15 ENDOR experiments employed a Davies echo-detected pulse sequence (42), inversion-T- $\pi/2$ - τ - π -
16
17 τ -acquire with the 9 μs radiofrequency pulse applied during the 10 μs T period. For ^{14}N spectra
18
19 the inversion pulse was 600 ns with $\pi = 120$ ns and $\tau = 600$ ns. For ^1H spectra the inversion pulse
20
21 was 400 ns with $\pi = 200$ ns and $\tau = 1000$ ns. The static field was 2650 G, $g = 2.61$. Each
22
23 spectrum is the sum of 600 scans. Further EPR spectra (under the same conditions) were
24
25 collected for a 100 μM DGCR8 sample and for a 100 μM CuSO_4 sample, to enable independent
26
27 determination of the DGCR8 concentration and its absorption coefficient in the UV-vis
28
29 spectrum.
30
31
32
33
34
35
36
37
38
39
40

41 ***Resonance Raman spectroscopic analysis of DGCR8. (i) Sample preparation.*** The
42
43 concentration of the ferric DGCR8 sample used was 85 μM in 50 mM Tris (pH 8.0), 500 mM
44
45 KCl plus 10% glycerol. The 50 μl ferric sample was transferred into an NMR tube for
46
47 measurements. The ferrous DGCR8, dissolved in the glycerol-containing buffer, was then
48
49 generated by first degassing the DGCR8 sample under O_2 -free nitrogen, before adding a 20-fold
50
51 molar excess of sodium dithionite and the redox mediators methyl viologen (MV) and benzyl
52
53 viologen (BV) to final concentrations of 0.3 μM and 1 μM , respectively; these additives being
54
55
56
57
58
59
60

1
2
3 dissolved in the same glycerol-containing buffer. Reduction of the hemoprotein was monitored
4
5 by electronic absorption spectrophotometry in the UV-vis region at 20°C, noting that full
6
7 reduction required up to one hour. The Fe^{II}-CO complex was then prepared by saturation of a
8
9 sample of DGCR8 with CO prior to the addition of dithionite and the BV and MV mediators (as
10
11 done for the ferrous, CO-free sample). Complete formation of the DGCR8 Fe^{II}-CO complex was
12
13 ensured by monitoring the electronic absorption spectrum. A second sample of ferric DGCR8
14
15 was prepared in glycerol-free buffer and studied in an effort to resolve an apparent conflict with
16
17 previous reports regarding spin-state populations (*vide infra*) (36). This second sample was
18
19 prepared by adding 50 µl of glycerol-free 50 mM Tris (pH 8.0), 500 mM KCl buffer to 50 µl of
20
21 the sample in the 10% glycerol-containing buffer contained in a centrifugal filter cartridge (10K
22
23 molecular weight cut-off), and by concentrating the 100 µl resulting solution to ~50 µl using a
24
25 microcentrifuge at 8000 rpm and 4°C. This process was repeated 8 times to ensure the buffer was
26
27 completely exchanged. **(ii) Resonance Raman measurements.** The ferric DGCR8 samples were
28
29 measured with the 441.6 nm excitation line from a He-Cd laser (IK Series He-Cd laser, Kimmon
30
31 Koha Co. Ltd., CO), while the ferrous DGCR8 sample was measured with the 415 nm line
32
33 provided by a Kr⁺ laser (Coherent Innova Sabre Ion Laser). The spectra of the Fe^{II}-CO adducts
34
35 were also acquired with the 441.6 nm line. The RR spectra of all samples were measured using a
36
37 Spex 1269 spectrometer equipped with a Spec-10 LN liquid nitrogen-cooled detector (Princeton
38
39 Instruments, NJ). The slit width was 150 µm, and the laser power was adjusted to ~30 mW at the
40
41 laser for the ferric and ferrous samples, while a power of ~1 mW was maintained for the CO
42
43 adducts to minimize photodissociation. All samples were measured in a spinning NMR tube to
44
45 avoid local heating and protein degradation. The spectra were collected using a 180°
46
47 backscattering geometry, and the laser power was focused on the sample with a line image using
48
49
50
51
52
53
54
55
56
57
58
59
60

1
2
3 a cylindrical lens. Spectra were calibrated with data acquired for fenchone and processed with
4 Grams/32 AI software (Galactic Industries, Salem, NH). Data were collected at 4 (\pm 2) $^{\circ}$ C by
5
6 placing the samples in a homemade quartz Dewar flask filled with cold water and monitoring
7
8 during the measurements using a thermocouple.
9
10
11

12 13 14 15 16 17 **RESULTS AND DISCUSSION**

18 19 20 *Expression and purification of human DGCR8*

21
22
23 The Δ 276 form of DGCR8 (26) was purified to homogeneity as described in *Experimental*
24 *Procedures*. Some nucleotide contamination (as evidenced by an absorbance feature at 260 nm)
25
26 was seen in the protein eluted from the nickel affinity column at a high (500 mM) imidazole
27
28 concentration, but this spectral feature was not observed for the portion of DGCR8 protein eluted
29
30 in 100 mM imidazole. Protein was further purified by heparin affinity and Sepharose S200 gel
31
32 filtration chromatography steps.
33
34
35
36
37
38
39
40
41

42 43 *UV-vis spectroscopic analysis of DGCR8*

44
45 In its oxidized (ferric) state, the purified DGCR8 hemoprotein has a hyperporphyrin UV-vis
46
47 absorption spectrum similar to that described previously (26), with the main Soret peak at 450
48
49 nm and the second feature at 367 nm. In the visible region, the ferric heme exhibits a broad
50
51 absorption feature with a peak at \sim 557 nm and a shoulder at \sim 586 nm (**Figure 1A**). In previous
52
53 studies on the cysteine thiolate-coordinated camphor hydroxylase P450cam by Sono *et al.*, the
54
55 P450 was titrated with the sulfur donor ligand *p*-chlorothiophenol, generating a ferric *bis*-Cys
56
57
58
59
60

1
2
3 heme ligated model complex, and resulting in the formation of a hyperporphyrin spectrum with
4
5 Soret maxima at 380 and 450 nm (43). Further studies on the binding of 1-propanethiol to
6
7 P450cam at pH 6.7 revealed three absorbance peaks in the Soret region at approximately 380
8
9 nm, 417 nm and 465 nm, indicative of a mixture of axial *bis*-thiolate (the 380 nm/465 nm bands)
10
11 and thiolate/thiol coordination (the 417 nm band). Increasing the pH resulted in the conversion of
12
13 the 1-propanethiol-bound species near-completely to the hyperporphyrin 380 nm/465 nm form at
14
15 pH 9.1, arising from the deprotonation of the distal ligand to the thiolate state (43). In studies
16
17 using porphyrin model complexes, Ullrich *et al.* also reported *bis*-thiolate complexes with split
18
19 Soret features and absorption maxima at ~470 nm and 380 nm (44). More recent studies with the
20
21 RDX (1,3,5-trinitroperhydro-1,3,5-triazine) explosive-degrading P450 XplA (CYP177A1)
22
23 showed that titration with dithiothreitol produced a mixture of *bis*-thiolate (the main species,
24
25 with maxima at ~374 nm/453 nm) and thiol-thiolate (423 nm) 6-coordinated forms. Similar
26
27 binding studies using β -mercaptoethanol show predominantly the thiol-thiolate form of XplA at
28
29 pH 6 (at ~420 nm). However, in more basic conditions (pH 8), the hyperporphyrin, *bis*-thiolate
30
31 spectrum dominates with maxima at ~372 nm/453 nm) (45). Comparison of the UV-vis spectrum
32
33 of ferric DGCR8 with these data suggests that heme coordination in DGCR8 occurs with
34
35 cysteines in their thiolate form providing both the proximal and distal ligands, in agreement with
36
37 published data (46). A DGCR8 absorption coefficient of $\epsilon_{450} = 70 \text{ mM}^{-1} \text{ cm}^{-1}$ was calculated for
38
39 its most intense heme absorbance band using the pyridine hemochromagen method (41). An
40
41 independent determination of the DGCR8 absorption coefficient ($70 \pm 2 \text{ mM}^{-1} \text{ cm}^{-1}$) was
42
43 obtained using X-band EPR with reference to the spectrum of a CuSO_4 standard and the UV-vis
44
45 absorbance spectrum of the same protein sample. This coefficient is consistent with an estimate
46
47 from Senturia *et al.* ($74 \text{ mM}^{-1} \text{ cm}^{-1}$ for the human NC1 and HBD constructs), and with the
48
49
50
51
52
53
54
55
56
57
58
59
60

1
2
3 frog/bat star (starfish) orthologs that have absorption coefficients of 72/70 $\text{mM}^{-1} \text{cm}^{-1}$,
4
5 respectively (47).
6
7
8
9
10

11 *DGCR8 heme ligation in the ferrous state*

12
13
14
15
16 Reduction of the ferric DGCR8 heme iron to the ferrous state (using the strong reductant sodium
17
18 dithionite, $E^\circ \sim -420 \text{ mV}$ vs. the normal hydrogen electrode, NHE) progressed slowly to
19
20 completion at 20°C; although the rate of heme reduction was enhanced on the addition of the
21
22 electron transfer mediators benzyl viologen (BV) and methyl viologen (MV), suggesting that
23
24 access of reductant to the protein-bound heme may be restricted. In an anaerobic environment in
25
26 the presence of BV and MV and with excess dithionite, the complete reduction of the ferric
27
28 DGCR8 heme iron occurs at 20°C over a period of approximately 10 minutes. In the reduced
29
30 (ferrous) form, DGCR8 exhibits a Soret maximum at 427 nm with absorbance bands in the
31
32 visible region at 531 and 559 nm. There is also an increase in the absorption coefficient for the
33
34 ferrous Soret band from $\epsilon_{450} = 70 \text{ mM}^{-1} \text{cm}^{-1}$ for the oxidized protein to $\epsilon_{427} = 112 \text{ mM}^{-1} \text{cm}^{-1}$ in
35
36 the reduced state (**Figure 1A**). Dawson's group made spectroscopic investigations of heme axial
37
38 coordination using a mutated myoglobin with no axial heme coordination from the polypeptide.
39
40 Using either cyclopentanethiol, to mimic *bis*-cysteine coordination (48), or imidazole to mimic
41
42 histidine coordination (49) they determined the spectroscopic properties of these complexes. In
43
44 both cases, the addition of the neutral ligand yields a UV-vis spectrum with properties similar to
45
46 that of the ferrous $\Delta 276$ DGCR8 protein, suggesting that, in the ferrous state, DGCR8 is
47
48 coordinated by neutral axial ligand or ligands, prospectively through CysH/CysH coordination.
49
50
51
52
53
54
55
56
57
58
59
60

1
2
3 In the ferrous state, the DGCR8 heme iron binds CO, producing a UV-vis spectrum with
4 a Soret maximum of substantially increased intensity at 422 nm ($\epsilon_{422} = 168 \text{ mM}^{-1} \text{ cm}^{-1}$) (**Figure**
5 **1A**). Once reduced to the ferrous state, binding of CO occurs rapidly, forming a complex which
6 remains stable for several hours in either an aerobic or anaerobic environment. In cytochrome
7 P450 enzymes (P450s), the binding of CO to the ferrous heme iron gives a characteristic Soret
8 band spectral shift to ~ 450 nm that results from cysteine thiolate coordination *trans* to the CO.
9 However, in various P450s the ferrous-CO complex can have a Soret feature at around 420 nm
10 (the P420 state), which is generally considered to be the species arising from protonation of the
11 proximal thiolate ligand to the thiol form (48). In favor of this conclusion are data such as the
12 reversible titration of P450 to P420 in the pH range from ~ 5 -9 for the *Mycobacterium*
13 *tuberculosis* CYP121A1 enzyme, and the rapid conversion of P450 to P420 in the *M.*
14 *tuberculosis* sterol demethylase CYP51B1, due to instability of the proximal thiolate to
15 protonation in the ferrous form of the enzyme (50-52). However, heme-binding proteins with an
16 axial histidine ligand to their heme iron also have a similar spectrum in their ferrous-CO bound
17 states (e.g. the hemoglobin Fe^{II} -CO complex has a Soret maximum at 420 nm). Indeed, it has
18 been proposed that in the P450s the cytochrome P420 form may result from a proximal ligand
19 switch from cysteine thiolate to a neutral histidine coordinated state (53). The absence of a Soret
20 band at 450 nm thus strongly suggests that in its ferrous, CO-bound state the DGCR8 heme iron
21 is not coordinated to the protein by a thiolate ligand, but instead via a neutral thiol or a histidine.
22 With reference to the aforementioned studies on P450 enzymes, the DGCR8 ferrous-CO
23 complex is most likely to have a cysteine thiol ligand *trans* to the CO. As described below, the
24 results from RR studies are also consistent with this conclusion.
25
26
27
28
29
30
31
32
33
34
35
36
37
38
39
40
41
42
43
44
45
46
47
48
49
50
51
52
53
54
55
56
57
58
59
60

1
2
3 The binding of nitric oxide (NO) was also investigated for both the ferrous and ferric
4 forms of DGCR8 under anaerobic conditions. In ferric DGCR8 no evidence of binding was seen,
5 consistent with DGCR8 being hexacoordinate in this oxidation state (four equatorial ligands
6 from heme pyrrole nitrogens and two axial ligands from DGCR8 amino acid side chains) and
7 with NO being unable to displace either axial ligand. In the ferrous heme iron state, the binding
8 of NO was investigated by stopped-flow UV-vis spectroscopy at 4 °C. One syringe contained
9 NO-saturated buffer (~1.9 mM) while the other contained ferrous DGCR8. As with ferric
10 DGCR8, no evidence was seen for a NO-bound form, but instead the collapse of the DGCR8
11 ferrous species to the ferric state was observed as a shift in the Soret maximum from 427 nm to
12 450 nm, with an isosbestic point (442 nm) between the two forms. These data suggest that a
13 short lived ferrous-NO species is formed transiently, but that it is unstable and rapidly decays to
14 form the ferric DGCR8 state in ~5 seconds. The binding of dioxygen (O₂) to the ferrous Δ276
15 DGCR8 was also explored in the same manner as done for NO binding. In this case, the
16 formation of an oxy-complex was observed, with a Soret maximum at 423 nm. However, this
17 species was also unstable, and converted rapidly back to the ferric resting state, likely by
18 dissociation of superoxide from the heme iron (**Figure 1B**).

19
20
21
22
23
24
25
26
27
28
29
30
31
32
33
34
35
36
37
38
39
40
41
42 In other studies, the UV-vis spectrum of the ferric form of DGCR8 was examined as a
43 function of temperature in the range between 20°C and -80°C. However, no significant spectral
44 shifts were observed for the ferric form. Similarly, the addition of freshly synthesized microRNA
45 (10 μM pri-miRNA added to 1.3 μM DGCR8) did not induce any perturbation to either the
46 DGCR8 ferric or ferrous heme spectrum. This suggests that while the HBD (along with the
47 dsRNA binding domains) is predicted to be crucial for productive interactions with the pri-
48 miRNAs, the substrate binding mode is not one that perturbs the heme ligation environment (32).

EPR and Electron-Nuclear Double Resonance (ENDOR) spectroscopy of DGCR8

Human DGCR8 in the ferric state gave rise to a rhombic EPR spectrum (**Figure 2A**) at 10 K with g -values of 2.61, 2.27 and 1.83. Such spectra are typical of low-spin ferric ($S = \frac{1}{2}$) hemes and the g -values fall within the range previously associated with low-spin hemes having a thiolate proximal axial ligand (54). A similar EPR spectrum has been reported for DGCR8 from frog (*Xenopus laevis*) (46).

Davies pulsed ENDOR spectra taken at a static field of 2650 G, $g = 2.61$, revealed two groups of lines. One group are symmetrical about the ^1H Larmor frequency at this field, 11.3 MHz, and arise from hyperfine coupling to ^1H nuclei (protons) (**Figure 2B**). The central feature of this spectrum originates from unresolved hyperfine couplings to protons distant from the heme iron (matrix protons) (55). A resolved hyperfine coupling of 5.1 MHz is also evident. Spectra collected using the same experimental parameters, but with a sample exchanged into D_2O solvent, reveal that some of the matrix protons are exchangeable, with the largest ^1H hyperfine coupling to such an exchangeable proton being 2.4 MHz. Exchangeable protons attached to atoms directly ligating the heme in the distal position, such as water or substrate protons, typically have hyperfine couplings of 8-12 MHz (56), protons of methylene groups *beta* to the ligating atom have been reported to exhibit hyperfine couplings of 5-7 MHz (57). The second group of lines are found at lower frequencies, are not symmetrical about the ^1H Larmor frequency and exhibit distinct differences in intensity. These lines arise from hyperfine coupling to ^{14}N nuclei (58) and are thus also subject to the effects of the ^{14}N quadrupolar interaction with the frequencies of the lines, ν_{\pm} , being described by:

$$\nu_{\pm} = |\nu_N \pm A/2 \pm 3P/2|$$

Here, ν_N is the ^{14}N nuclear Larmor frequency, 0.81 MHz, A is the hyperfine coupling and $3P$ is the quadrupole splitting). Taking lines of the same intensity as coming from the same spin manifold provides the assignment of those lines shown in **Figure 2C**. Only one hyperfine coupling of 6.3 MHz and one quadrupolar interaction, with quadrupolar splitting $3P = 0.95$ MHz, are evident. Such values are typical for hyperfine coupling to the pyrrole nitrogens in low-spin ferric hemes with neutral distal ligands, since the quadrupolar splitting is sensitive to the presence of charged ligands, when observed along the normal to the heme plane (59). The small linewidths evident in **Figure 2C** support such an orientation for the g axis associated with $g = 2.61$. However, the detection of only one hyperfine coupling for all four pyrrole nitrogens is relatively unusual and suggests very high symmetry around the heme normal (60). Such symmetry has been observed for P450s with a thiolate proximal axial ligand and a neutral distal axial ligand, and in model compounds with two identical axial ligands (61). There is no evidence for hyperfine coupling to a ^{14}N atom from an axial ligand.

Taken together, these ENDOR data exclude water and histidine as ligands to the heme iron due to the lack of a large hyperfine coupling to an exchangeable proton (or protons) and any ^{14}N hyperfine coupling beyond that to the pyrrole nitrogens. The 0.95 MHz quadrupole splitting suggests a neutral proximal ligand, such as a thiol (although ENDOR cannot distinguish between sulfur and oxygen without isotope labelling), However, the lack of a hyperfine coupling to an exchangeable proton large enough be attributed to the -SH group proton argues against this and suggests a thiolate distal axial ligand. The observation of a single ^{14}N hyperfine coupling indicates an unusually high symmetry along the normal to the heme plane and therefore supports

1
2
3 the latter model with two identical axial ligands. Thus, while the ENDOR data are equivocal they
4
5 provide strongest support for *bis*-thiolate heme ligation in ferric DGCR8.
6
7
8
9

10 11 12 ***Resonance Raman spectroscopy of DGCR8.*** 13

14
15
16 **(i) Ferric DGCR8.** The high frequency region of the ferric DGCR8 sample is presented in
17
18 **Figure 3A.** The region includes the oxidation state and spin-state markers. The high frequency
19
20 spectrum of the DGCR8 sample exhibits the oxidation state marker mode, ν_4 , at 1375 cm^{-1} and
21
22 the ν_3 spin-state marker at 1506 cm^{-1} , confirming the presence of a ferric 6-coordinate low-spin
23
24 state, in agreement with results from other methods used in this study. While there are some
25
26 small differences ($3\text{-}6\text{ cm}^{-1}$) in frequencies between our results and those reported in the earlier
27
28 published data from Barr *et al.* (36), they can be attributed to the one-point spectral calibration
29
30 method used in the published work compared to the multipoint calibration used in the present
31
32 studies. Slight differences in relative intensities of bands between the two studies are attributable
33
34 to the fact that two different excitation lines were used (441.6 in this study, 457.9 nm in the
35
36 previous study). In the previous study, a weak 1471 cm^{-1} band was taken as evidence for a 5-
37
38 coordinate high-spin component. In our study, a band is also observed near this frequency (1465
39
40 cm^{-1} , **Figure 3A**) but is assigned to an internal mode of glycerol, whose concentration is 10%
41
42 (volume/volume) in our sample. The DGCR8 samples analyzed by Barr *et al.* also contained
43
44 10% glycerol (36). In order to verify the assignment of this 1465 cm^{-1} feature to glycerol, further
45
46 experiments were conducted on a DGCR8 sample containing no glycerol. The inset in **Figure**
47
48 **3A** shows spectra of the ferric DGCR8 sample containing 10% glycerol buffer (a), a sample in
49
50 the same buffer without glycerol (b), and their difference spectrum (c). In the difference
51
52
53
54
55
56
57
58
59
60

1
2
3 spectrum, all the heme modes were cleanly cancelled out, revealing only the 1465 cm⁻¹ glycerol
4 band. Thus, we assigned this band to the 10% glycerol present in the original protein solution,
5 confirming the interpretation that the ferric protein samples studied here contain an insignificant
6 amount of a 5-coordinate HS state. The low frequency region of the RR spectrum is shown in
7
8 **Figure S1A** of the Supporting Information.
9
10
11
12
13

14
15
16 **(ii) Ferrous DGCR8.** In the ferrous state, the high-frequency region (**Figure 3B**)
17 exhibited the oxidation state marker band (ν_4) at 1362 cm⁻¹ and the spin-state marker band (ν_3) at
18 1495 cm⁻¹, indicating a low-spin 6-coordinated ferrous heme protein. Again, the weak broad
19 glycerol band near 1465 cm⁻¹ was observed. In the previous study, a 1470 cm⁻¹ band was
20 observed and assigned to the ν_3 mode of a 5-coordinate HS component, again prompting the
21 conclusion of a mixture of 5- and 6-coordinate forms of the ferrous DGCR8, as was also reported
22 in that work for DGCR8 in the ferric state (36). While that 1470 cm⁻¹ feature is reasonably close
23 to the expected glycerol band, the frequency observed is slightly higher than expected.
24 Considering it not to be a miscalibrated glycerol band, the authors assigned it to the ν_3 mode of a
25 HS component, also assigning a feature at 1579 cm⁻¹ to the ν_2 mode of that HS component.
26 However, this frequency is unusually high for a HS component. Assuming that the 1470 cm⁻¹
27 feature observed by Barr *et al.* does provide confirmation of a HS component, this would suggest
28 that the sample studied previously (frog DGCR8, amino acids 278-498) does form a HS
29 component, while the isoform studied here (human DGCR8, amino acids 276-773) does not form
30 a HS species under our conditions. The low-frequency RR spectrum of ferrous DGCR8 is shown
31 in **Figure S1B** of the Supporting Information.
32
33
34
35
36
37
38
39
40
41
42
43
44
45
46
47
48
49
50
51
52

53
54
55 **(iii) Ferrous-CO complex of DGCR8.** As discussed above, the appearance of a Soret
56 band near 420 nm for the ferrous CO adduct of DGCR8 is indicative of a 6-coordinate CO-
57
58
59
60

1
2
3
4
5
6
7
8
9
10
11
12
13
14
15
16
17
18
19
20
21
22
23
24
25
26
27
28
29
30
31
32
33
34
35
36
37
38
39
40
41
42
43
44
45
46
47
48
49
50
51
52
53
54
55
56
57
58
59
60

ligated heme bearing a neutral (e.g., thiol or histidine) *trans*-axial ligand. Resonance Raman spectra in the region between 1000-1650 cm^{-1} , provided in **Figure S1C** of the Supporting Information, reveal the oxidation state marker band (ν_4) at 1373 cm^{-1} and the spin-state marker band (ν_3) at 1497 cm^{-1} , consistent with values typically seen for these low-spin CO adducts of cytochromes P450 (62, 63). The regions of the RR spectra for the Fe^{II} -CO and Fe^{II} - ^{13}C CO adducts of DGCR8, wherein the $\nu(\text{Fe-C})$ and $\nu(\text{C-O})$ stretching modes occur, are shown in **Figure 3C**. In the lower frequency region a clean difference pattern emerges from a $\nu(\text{Fe-}^{12}\text{C})$ mode appearing at 496 cm^{-1} , with its ^{13}C counterpart shifting to 490 cm^{-1} . The corresponding $\nu(\text{C-O})$ bands appear at 1963 cm^{-1} for $^{12}\text{C-O}$ and at 1917 cm^{-1} for the ^{13}C analogue. Finally, a clean difference pattern, with components at 575 and 557 cm^{-1} , reveal the $\delta(\text{Fe-C-O})$ bending mode.

Figure 3D shows the well-established inverse correlation plots for $\nu(\text{Fe-C})$ vs $\nu(\text{C-O})$ modes, which are useful for probing the nature of the distal heme pockets and proximal ligands (64). Thus, the lowest line in the figure includes data for the cytochromes P450, which possess a strongly electron donating thiolate proximal ligand, leading to relatively high $\nu(\text{Fe-S})$ stretching modes occurring near 350-355 cm^{-1} . Just above this line lies the correlation plot for NOS enzymes; possessing lower $\nu(\text{Fe-S})$ frequencies (337-343 cm^{-1}), these show correspondingly higher $\nu(\text{Fe-C})$ stretching modes. Highest in the figure is the correlation line for histidine bound Fe^{II} -CO complexes. As was discussed above, protonation of the *trans*-axial thiolate to form a *trans* thiol-ligated species, as suggested for cytochromes P420 (65), would lead to an even weaker Fe-S bond and higher $\nu(\text{Fe-C})$ stretching frequencies, compared to those seen for NOS adducts. Indeed, the points acquired for the P420 forms of iNOS and for CYP101A1 (the camphor hydroxylase P450cam) (66), as well as one for a well-characterized CO adduct of a heme model compound bearing a *trans*-axial thiol (67), lie near the line corresponding to

1
2
3 histidine-ligated CO adducts. The point determined herein for the CO adduct of DGCR8 clearly
4
5 lies in the neighborhood of those adducts bearing a *trans*-axial thiol ligand, a result which is
6
7 consistent with the conclusion that the ferrous form of the enzyme possesses a thiol/thiol
8
9 coordination environment.
10
11

12 13 14 15 16 17 ***Magnetic Circular Dichroism (MCD) spectroscopy of DGCR8*** 18

19
20 The continuous wave (CW) EPR spectrum of $\Delta 276$ DGCR8 contains sharp features with
21
22 principal *g*-values of 2.61, 2.27 and 1.83, confirming that the ferric heme iron is almost
23
24 exclusively in the low-spin state. For *b*-type cytochromes, such a spectrum is diagnostic of axial
25
26 ligation by thiolate. To provide further insights into the nature of the second axial ligand to the
27
28 DGCR8 heme iron we used MCD as a complementary spectroscopic method (54).
29
30
31

32
33 **Figure 4** shows MCD spectra for ferric DGCR8 in UV-vis and near-infrared (NIR)
34
35 regions, and for ferrous DGCR8 in the UV-vis region. **Figure 4A** shows the UV-vis MCD
36
37 spectrum for ferric DGCR8 with a Soret derivative at 451 nm and a Q-band region derivative at
38
39 556 nm. NIR MCD spectroscopy of low-spin ferric heme affords a direct measurement of the
40
41 porphyrin-to-iron LMCT (ligand-to-metal charge transfer) transition and often this is sufficient
42
43 to allow unambiguous assignment of axial ligation (68). **Figure 4B** shows the MCD spectrum of
44
45 ferric DGCR8. The charge transfer band in the NIR region is located at 1260 nm, outside the
46
47 range reported for heme with Cys⁻/H₂O or Cys⁻/His as axial ligands (1050-1200 nm) (69-71).
48
49 This observation, together with the assignment of Cys⁻ ligation based on the CW EPR, suggests
50
51 an unusual *trans*-axial ligand to the DGCR8 ferric heme iron. Based on conclusions from other
52
53 spectroscopic analyses reported here, we would favor cysteine thiolate as the *trans*-axial ligand.
54
55
56
57
58
59
60

1
2
3 However, a *trans*-thiol ligand might also be possible. In favor of the assignment of *bis*-thiolate
4 coordination in ferric DGCR8, the UV-vis MCD spectrum of DGCR8 contains an unusual
5 negative band at 597 nm, in addition to the derivative features at 451 and 556 nm typical of ferric
6 heme. A highly similar UV-vis MCD spectrum is seen for the cysteine thiolate-coordinated,
7
8 ferric heme iron form of the *Caldariomyces fumago* chloroperoxidase (CPO) in complex with
9
10 methanethiol (72). UV-vis absorbance analysis of the CPO/methanethiol complex shows a clear
11
12 hyperporphyrin spectrum, consistent with *bis*-thiolate heme ligation (72). Thus, we conclude
13
14 from these MCD studies that the heme of DGCR8 is indeed ligated by two cysteine residues in
15
16 the ferric state, with both these residues in their thiolate form.
17
18
19
20
21
22
23
24

25
26 In contrast to the readily observed NIR MCD bands of low-spin ferric hemes, the
27
28 corresponding LMCT transitions for ferrous hemes are symmetry forbidden, precluding ligand
29
30 assignment for reduced hemes on this basis. However, the form of the UV-vis MCD in the
31
32 reduced state can be used to confirm ligation by cysteinate, as this gives an abnormally low
33
34 intensity α,β band with peak-to-trough intensity of $\sim 70 \text{ M}^{-1} \text{ cm}^{-1} \text{ T}^{-1}$ (73). UV-vis MCD spectra
35
36 were collected for reduced DGCR8 (**Figure 4C**). Sodium dithionite reductant was added to the
37
38 sample under anaerobic conditions and UV-vis absorbance and MCD spectra were collected after
39
40 4 hours at 20°C. Following data collection, it became apparent that a small proportion of the
41
42 enzyme had reoxidized ($\sim 15\%$). To account for the partial reoxidation, the spectra were corrected
43
44 by removal of the small spectral contribution from the ferric enzyme (with reference to the UV-
45
46 vis absorption and MCD spectra of the ferric DGCR8) to produce the ferrous DGCR8 spectra
47
48 without significant contribution from the ferric species. The calculated UV-vis MCD spectrum of
49
50 reduced DGCR8 (**Figure 4C**) has a much greater intensity in this region, approximately 350 M^{-1}
51
52 $\text{cm}^{-1} \text{ T}^{-1}$. Furthermore, this band is located at 556 nm with the maximum Soret intensity at 436
53
54
55
56
57
58
59
60

1
2
3 nm, in contrast with the 550 and 416 nm bands, respectively, observed for SoxAX, an enzyme
4 that couples disulfide bond formation to cytochrome *c* reduction in a widespread microbial sulfur
5 oxidation pathway and which has the more common Cys⁻/His ligand set (73). Both the intensity
6 and position of the UV-vis MCD bands of reduced DGCR8 show far greater similarity to those
7 of the reduced form of a model complex with *bis*-thiol ligation (α,β intensity $220 \text{ M}^{-1} \text{ cm}^{-1} \text{ T}^{-1}$ at
8 555 nm, Soret band at $>430 \text{ nm}$) (48). Thus, whilst the form of the MCD spectrum does not
9 preclude displacement of Cys⁻ by a neutral ligand (such as His-imidazole) upon reduction, it is
10 also consistent with protonation of this residue resulting in a CysH/CysH coordinated ferrous
11 heme.
12
13
14
15
16
17
18
19
20
21
22
23
24
25
26
27
28

29 CONCLUSIONS

30
31
32 DGCR8 is an unusual hemoprotein with distinctive spectroscopic features to other heme *b*-
33 binding proteins. Binding of heme to the DGCR8 dimer stabilizes the protein and the DGCR8
34 dimer forms a complex with the RNase Drosha that is crucial for pri-miRNA processing (46, 74,
35 75). Our combined spectroscopic studies identify axial coordination of DGCR8 by two sulfur-
36 containing amino acids in both its ferric and ferrous states. Data are consistent with Cys⁻/Cys⁻
37 (*bis*-thiolate) axial coordination of the ferric DGCR8 heme *b*, but indicate that ferrous DGCR8
38 likely adopts CysH/CysH (*bis*-thiol) ligation. Addition of pri-miRNA substrate to the (active)
39 ferric DGCR8 form does not perturb its heme spectrum, suggesting that the pri-miRNA binding
40 site does not overlap the heme site, even though recent studies indicate that portions of the HBD
41 are crucial for interactions with pri-miRNA (32).
42
43
44
45
46
47
48
49
50
51
52
53
54
55
56
57
58
59
60

1
2
3 The rhombic EPR spectrum of low-spin ferric DGCR8 indicates a single dominant axial
4 ligation mode (**Figure 2A**). Cys352 was proposed as an axial ligand to the heme iron, and
5 modelling suggests that Cys352 thiolates from two monomers of the HBD act as axial ligands to
6 a hexacoordinated DGCR8 heme iron at the dimer interface (36). Spectroscopic analyses
7 presented in this paper are consistent with *bis*-Cys coordination of DGCR8 heme iron. In
8 particular, our ENDOR data for ferric DGCR8 confirm a highly symmetrical heme coordination
9 environment and rule out water or histidine as axial ligands, instead favoring a Cys⁻/Cys⁻ axial
10 ligand pair. The $\Delta 276$ DGCR8 hemoprotein is reduced by dithionite to produce a species with a
11 Soret band shift to 427 nm, similar to that for the reduced frog DGCR8 HBD form. However, the
12 absorption coefficient reported for the ferrous frog HBD ($\epsilon_{424} = 55 \text{ mM}^{-1} \text{ cm}^{-1}$) is much lower
13 than that we report here for ferrous human DGCR8 (36). The Soret coefficient is $\epsilon_{450} = 70 \text{ mM}^{-1}$
14 cm^{-1} for ferric human DGCR8, while that for the ferrous DGCR8 is considerably higher at $\epsilon_{427} =$
15 $112 \text{ mM}^{-1} \text{ cm}^{-1}$. The DGCR8 ferrous-CO complex has an even more intense Soret feature ($\epsilon_{421} =$
16 $168 \text{ mM}^{-1} \text{ cm}^{-1}$) (**Figure 1A**). The absorption coefficient for the P420 ferrous-CO (thiol-
17 coordinated) form of cytochrome P450 enzymes is also larger than that for the P450 (thiolate-
18 coordinated) form, consistent with the presence of a cysteine thiol ligand *trans* to the CO in the
19 DGCR8 complex (76).

20
21
22
23
24
25
26
27
28
29
30
31
32
33
34
35
36
37
38
39
40
41
42
43
44
45
46
47
48
49
50
51
52
53
54
55
56
57
58
59
60
Barr *et al.* concluded that the ferrous frog HBD does not have cysteine thiolate
coordination. This is consistent with our data that indicate ferrous human DGCR8 has
CysH/CysH coordination. However, their conclusion that multiple spin and/or heme iron
coordination states are present is not supported by our ferrous DGCR8 spectroscopic data. Barr
et al. reported spectra for the human NC1 form of DGCR8 reduced by 2 mM dithionite at pH
6.0. However, the heme spectrum appears extensively bleached with substantial contributions

1
2
3 from dithionite and is devoid of any clear Soret feature at ~427 nm (36). These data are in
4
5 marked contrast to our UV-vis data for human DGCR8, where well defined ferrous (and Fe^{II}-
6
7 CO) spectra are observed. We attempted to determine the human DGCR8 redox potential using
8
9 spectroelectrochemistry, as described previously (52, 77). Aggregation of DGCR8 occurred over
10
11 the course of the experiment, preventing accurate estimation of the midpoint potential for the
12
13 heme Fe^{III}/Fe^{II} couple. However, the data clearly showed that the DGCR8 heme iron potential is
14
15 lower than -350 mV versus NHE. This suggests that ferric DGCR8 predominates under cellular
16
17 conditions, consistent with ferric DGCR8 being the active species in pri-miRNA processing (36).
18
19
20
21
22

23 Our UV-vis MCD spectrum for ferric human DGCR8 displays similar features to those
24
25 for frog DGCR8 HBD, but provides sharper resolution of bands, particularly in the α/β (Q) band
26
27 and LMCT regions (**Figure 4A**) (46). This enables identification of an unusual negative band at
28
29 597 nm, and its assignment to *bis*-cysteine thiolate ferric heme iron coordination by comparison
30
31 to a highly similar spectrum for the methanethiol complex of CPO, and with reference to the
32
33 near-complete hyperporphyrin UV-vis spectrum for the same complex (72). We also present the
34
35 first MCD data for a ferric DGCR8 protein in the NIR region, and for ferrous DGCR8 in the UV-
36
37 vis region. From the ferric NIR data set, the novel Cys⁻/Cys⁻ assignment is associated with the
38
39 unusual position of the MCD NIR CT band at 1260 nm. The well-defined ferrous DGCR8 UV-
40
41 vis MCD spectrum has much greater intensity than the ferric DGCR8 spectrum, and resembles
42
43 that of a *bis*-thiol coordinated model complex (48). This observation, along with RR data for
44
45 Fe^{II}-CO DGCR8, is consistent with CysH/CysH coordination of ferrous DGCR8, as opposed to
46
47 displacement of the axial ligand(s) or their replacement by undefined ligands, as suggested
48
49 previously (36).
50
51
52
53
54
55
56
57
58
59
60

1
2
3 In conclusion, we present detailed analyses of heme binding in the pre-miRNA
4 processing protein DGCR8. Assignments of heme coordination are made from spectroscopic
5 studies of human DGCR8 in both ferric/ferrous states. Contrary to previous work (36), we assign
6 the axial ligands as Cys⁻/Cys⁻ in active, ferric DGCR8, and as CysH/CysH in ferrous DGCR8,
7 with Cys352 residues from each monomer of a HBD domain dimer providing the sulfur thiolate
8 or thiol axial ligands.
9
10
11
12
13
14
15
16
17
18
19
20
21

22 **ACKNOWLEDGEMENTS.** The authors acknowledge Dr. Mark Dunstan (University of
23 Manchester) for assistance in RNA preparation, and Mrs Marina Golovanova (University of
24 Manchester) for assistance with protein expression.
25
26
27
28
29
30
31
32

33 **AUTHOR INFORMATION**

34
35
36
37 **Funding.** This research was supported through funding from the UK Biotechnology and
38 Biological Sciences Research Council (BBSRC grant number BB/F014252/1) to AWM, and by a
39 grant from the National Science Foundation (MCB 0951115) to JRK.
40
41
42
43
44

45 **Author Contributions.** The manuscript was written through contributions of all authors. All
46 authors have given approval to the final version of the manuscript.
47
48
49

50 **Supporting Information.** Additional Resonance Raman (RR) spectra for the ferric, ferrous and
51 ferrous-CO forms of the human DGCR8 protein. This material is available free of charge via the
52 Internet at <http://pubs.acs.org>.
53
54
55
56
57
58
59
60

REFERENCES

1. Krol, J., Loedige, I., and Filipowicz, W. (2010) The widespread regulation of microRNA biogenesis, function and decay, *Nat. Rev. Genet.* *11*, 597-610.
2. Llave, C., Xie, Z. X., Kasschau, K. D., and Carrington, J. C. (2002) Cleavage of Scarecrow-like mRNA targets directed by a class of Arabidopsis miRNA, *Science* *297*, 2053-2056.
3. Olsen, P. H., and Ambros, V. (1999) The lin-4 regulatory RNA controls developmental timing in *Caenorhabditis elegans* by blocking LIN-14 protein synthesis after the initiation of translation, *Dev. Biol.* *216*, 671-680.
4. Yekta, S., Shih, I. H., and Bartel, D. P. (2004) MicroRNA-directed cleavage of HOXB8 mRNA, *Science* *304*, 594-596.
5. Zeng, Y., Wagner, E. J., and Cullen, B. R. (2002) Both natural and designed micro RNAs technique can inhibit the expression of cognate mRNAs when expressed in human cells, *Mol. Cell.* *9*, 1327-1333.
6. Cai, X. Z., Hagedorn, C. H., and Cullen, B. R. (2004) Human microRNAs are processed from capped, polyadenylated transcripts that can also function as mRNAs, *RNA* *10*, 1957-1966.
7. Lee, Y., Kim, M., Han, J. J., Yeom, K. H., Lee, S., Baek, S. H., and Kim, V. N. (2004) MicroRNA genes are transcribed by RNA polymerase II, *EMBO J.* *23*, 4051-4060.
8. Zeng, Y., and Cullen, B. R. (2005) Efficient processing of primary microRNA hairpins by drosha requires flanking nonstructured RNA sequences, *J. Biol. Chem.* *280*, 27595-27603.
9. Lee, Y., Jeon, K., Lee, J. T., Kim, S., and Kim, V. N. (2002) MicroRNA maturation: stepwise processing and subcellular localization, *EMBO J.* *21*, 4663-4670.
10. Lund, E., Guttinger, S., Calado, A., Dahlberg, J. E., and Kutay, U. (2004) Nuclear export of microRNA precursors, *Science* *303*, 95-98.
11. Lee, Y., Ahn, C., Han, J. J., Choi, H., Kim, J., Yim, J., Lee, J., Provost, P., Radmark, O., Kim, S., and Kim, V. N. (2003) The nuclear RNase III Drosha initiates microRNA processing, *Nature* *425*, 415-419.
12. Denli, A. M., Tops, B. B. J., Plasterk, R. H. A., Ketting, R. F., and Hannon, G. J. (2004) Processing of primary microRNAs by the Microprocessor complex, *Nature* *432*, 231-235.
13. Gregory, R. I., Yan, K. P., Amuthan, G., Chendrimada, T., Doratotaj, B., Cooch, N., and Shiekhattar, R. (2004) The Microprocessor complex mediates the genesis of microRNAs, *Nature* *432*, 235-240.
14. Han, J. J., Lee, Y., Yeom, K. H., Kim, Y. K., Jin, H., and Kim, V. N. (2004) The Drosha-DGCR8 complex in primary microRNA processing, *Genes Dev.* *18*, 3016-3027.
15. Landthaler, M., Yalcin, A., and Tuschl, T. (2004) The human DiGeorge syndrome critical region gene 8 and its *D-melanogaster* homolog are required for miRNA biogenesis, *Current Biology* *14*, 2162-2167.
16. Bernstein, E., Caudy, A. A., Hammond, S. M., and Hannon, G. J. (2001) Role for a bidentate ribonuclease in the initiation step of RNA interference, *Nature* *409*, 363-366.
17. Hutvagner, G., McLachlan, J., Pasquinelli, A. E., Balint, E., Tuschl, T., and Zamore, P. D. (2001) A cellular function for the RNA-interference enzyme Dicer in the maturation of the let-7 small temporal RNA, *Science* *293*, 834-838.

- 1
 - 2
 - 3
 - 4
 - 5
 - 6
 - 7
 - 8
 - 9
 - 10
 - 11
 - 12
 - 13
 - 14
 - 15
 - 16
 - 17
 - 18
 - 19
 - 20
 - 21
 - 22
 - 23
 - 24
 - 25
 - 26
 - 27
 - 28
 - 29
 - 30
 - 31
 - 32
 - 33
 - 34
 - 35
 - 36
 - 37
 - 38
 - 39
 - 40
 - 41
 - 42
 - 43
 - 44
 - 45
 - 46
 - 47
 - 48
 - 49
 - 50
 - 51
 - 52
 - 53
 - 54
 - 55
 - 56
 - 57
 - 58
 - 59
 - 60
18. Ketting, R. F., Fischer, S. E. J., Bernstein, E., Sijen, T., Hannon, G. J., and Plasterk, R. H. A. (2001) Dicer functions in RNA interference and in synthesis of small RNA involved in developmental timing in *C-elegans*, *Genes Dev.* *15*, 2654-2659.
19. Khvorovova, A., Reynolds, A., and Jayasena, S. D. (2003) Functional siRNAs and rniRNAs exhibit strand bias, *Cell* *115*, 209-216.
20. Schwarz, D. S., Hutvagner, G., Du, T., Xu, Z. S., Aronin, N., and Zamore, P. D. (2003) Asymmetry in the assembly of the RNAi enzyme complex, *Cell* *115*, 199-208.
21. Czech, B., Zhou, R., Erlich, Y., Brennecke, J., Binari, R., Villalta, C., Gordon, A., Perrimon, N., and Hannon, G. J. (2009) Hierarchical rules for Argonaute loading in *Drosophila*, *Mol. Cell.* *36*, 445-456.
22. Ghildiyal, M., Xu, J., Seitz, H., Weng, Z., and Zamore, P. D. (2010) Sorting of *Drosophila* small silencing RNAs partitions microRNA* strands into the RNA interference pathway, *RNA* *16*, 43-56.
23. Okamura, K., Liu, N., and Lai, E. C. (2009) Distinct mechanisms for microRNA strand selection by *Drosophila* Argonautes, *Mol. Cell.* *36*, 431-444.
24. Yang, J. S., and Lai, E. C. (2011) Alternative miRNA Biogenesis Pathways and the Interpretation of Core miRNA Pathway Mutants, *Mol. Cell.* *43*, 892-903.
25. Sohn, S. Y., Bae, W. J., Kim, J. J., Yeom, K.-H., Kim, V. N., and Cho, Y. (2007) Crystal structure of human DGCR8 core, *Nat. Struct. Mol. Biol.* *14*, 847-853.
26. Faller, M., Matsunaga, M., Yin, S., Loo, J. A., and Guo, F. (2007) Heme is involved in microRNA processing, *Nat. Struct. Mol. Biol.* *14*, 23-29.
27. Senturia, R., Faller, M., Yin, S., Loo, J. A., Cascio, D., Sawaya, M. R., Hwang, D., Clubb, R. T., and Guo, F. (2010) Structure of the dimerization domain of DiGeorge Critical Region 8, *Protein Sci.* *19*, 1354-1365.
28. Yeom, K. H., Lee, Y., Han, J. J., Suh, M. R., and Kim, V. N. (2006) Characterization of DGCR8/Pasha, the essential cofactor for Drosha in primary miRNA processing, *Nucleic Acids Res.* *34*, 4622-4629.
29. Pickering, B. F., Yu, D. H., and Van Dyke, M. W. (2011) Nucleolin protein interacts with Microprocessor complex to affect biogenesis of microRNAs 15a and 16, *J. Biol. Chem.* *286*, 44095-44103.
30. Suzuki, H. I., Yamagata, K., Sugimoto, K., Iwamoto, T., Kato, S., and Miyazono, K. (2009) Modulation of microRNA processing by p53, *Nature* *460*, 529-U111.
31. Weitz, S. H., Gong, M., Barr, I., Weiss, S., and Guo, F. (2014) Processing of microRNA primary transcripts requires heme in mammalian cells, *Proc Natl Acad Sci U S A* *111*, 1861-1866.
32. Quick-Cleveland, J., Jacob, J. P., Weitz, S. H., Shoffner, G., Senturia, R., and Guo, F. (2014) The DGCR8 RNA-binding heme domain recognizes primary microRNAs by clamping the hairpin, *Cell Rep* *7*, 1994-2005.
33. Munro, A. W., Girvan, H. M., Mason, A. E., Dunford, A. J., and McLean, K. J. (2013) What makes a P450 tick?, *Trends Biochem. Sci.* *38*, 140-150.
34. Girvan, H. M., and Munro, A. W. (2013) Heme sensor proteins, *J. Biol. Chem.* *288*, 13194-13203.
35. Roberts, G. P., Thorsteinsson, M. V., Kerby, R. L., Lanzilotta, W. N., and Poulos, T. (2001) CooA: a heme-containing regulatory protein that serves as a specific sensor of both carbon monoxide and redox state, *Prog. Nucleic Acid Res. Mol. Biol.* *67*, 35-63.

- 1
- 2
- 3
- 4 36. Barr, I., Smith, A. T., Chen, Y. Q., Senturia, R., Burstyn, J. N., and Guo, F. (2012) Ferric, not ferrous, heme activates RNA-binding protein DGCR8 for primary microRNA processing, *Proc. Natl. Acad. Sci. U. S. A.* *109*, 1919-1924.
- 5
- 6
- 7 37. Kozomara, A., and Griffiths-Jones, S. (2011) miRBase: integrating microRNA annotation and deep-sequencing data, *Nucleic Acids Res* *39*, D152-D157.
- 8
- 9 38. Walker, S. C., Avis, J. M., and Conn, G. L. (2003) General plasmids for producing RNA in vitro transcripts with homogeneous ends, *Nucleic Acids Res.* *31*, e82.
- 10
- 11 39. Gurevich, V. V. (1996) Use of bacteriophage RNA polymerase in RNA synthesis, In *Viral Polymerases and Related Proteins*, pp 382-397, Academic Press Inc, San Diego.
- 12
- 13 40. Sambrook, J., and Russell, D. W. (2001) *Molecular Cloning - A Laboratory Manual*, 3rd ed., Cold Spring Harbor Laboratory Press, Cold Spring Harbor.
- 14
- 15 41. Berry, E. A., and Trumpower, B. L. (1987) Simultaneous determination of hemes-a, hemes-B, and hemes-C from pyridine hemochrome spectra, *Anal Biochem* *161*, 1-15.
- 16
- 17 42. Davies, E. R. (1974) New pulse ENDOR technique, *Phys. Lett. A* *47*, 1-2.
- 18
- 19 43. Sono, M., Andersson, L. A., and Dawson, J. H. (1982) Sulfur donor ligand-binding to ferric cytochrome-P-450-cam and myoglobin. Ultraviolet-visible absorption, magnetic circular dichroism, and electron-paramagnetic resonance spectroscopy investigation of the complexes, *J. Biol. Chem.* *257*, 8308-8320.
- 20
- 21 44. Ullrich, V., Nastainczyk, W., and Ruf, H. H. (1975) Ligand reactions of cytochrome P-450, *Biochem Soc Trans* *3*, 803-807.
- 22
- 23 45. Bui, S. H., McLean, K. J., Cheesman, M. R., Bradley, J. M., Rigby, S. E., Levy, C. W., Leys, D., and Munro, A. W. (2012) Unusual spectroscopic and ligand binding properties of the cytochrome P450-flavodoxin fusion enzyme XplA, *J. Biol. Chem.* *287*, 19699-19714.
- 24
- 25 46. Barr, I., Smith, A. T., Senturia, R., Chen, Y. Q., Scheidemantle, B. D., Burstyn, J. N., and Guo, F. (2011) DiGeorge critical region 8 (DGCR8) is a double-cysteine-ligated heme protein, *J. Biol. Chem.* *286*, 16716-16725.
- 26
- 27 47. Senturia, R., Laganowsky, A., Barr, I., Scheidemantle, B. D., and Guo, F. (2012) Dimerization and heme binding are conserved in amphibian and starfish homologues of the microRNA processing protein DGCR8, *PLoS One* *7*, e39688.
- 28
- 29 48. Perera, R., Sono, M., Sigman, J. A., Pfister, T. D., Lu, Y., and Dawson, J. H. (2003) Neutral thiol as a proximal ligand to ferrous heme iron: Implications for heme proteins that lose cysteine thiolate ligation on reduction, *Proc. Natl. Acad. Sci. U. S. A.* *100*, 3641-3646.
- 30
- 31 49. Du, J., Sono, M., and Dawson, J. H. (2011) The H93G myoglobin cavity mutant as a versatile scaffold for modeling heme iron coordination structures in protein active sites and their characterization with magnetic circular dichroism spectroscopy, *Coord. Chem. Rev.* *255*, 700-716.
- 32
- 33 50. Aoyama, Y., Horiuchi, T., Gotoh, O., Noshiro, M., and Yoshida, Y. (1998) CYP51-like gene of Mycobacterium tuberculosis actually encodes a P450 similar to eukaryotic CYP51, *J. Biochem.* *124*, 694-696.
- 34
- 35 51. Dunford, A. J., McLean, K. J., Sabri, M., Seward, H. E., Heyes, D. J., Scrutton, N. S., and Munro, A. W. (2007) Rapid P450 heme iron reduction by laser photoexcitation of Mycobacterium tuberculosis CYP121 and CYP51B1 - Analysis of CO complexation reactions and reversibility of the P450/P420 equilibrium, *J. Biol. Chem.* *282*, 24816-24824.
- 36
- 37
- 38
- 39
- 40
- 41
- 42
- 43
- 44
- 45
- 46
- 47
- 48
- 49
- 50
- 51
- 52
- 53
- 54
- 55
- 56
- 57
- 58
- 59
- 60

- 1
2
3
4
5
6
7
8
9
10
11
12
13
14
15
16
17
18
19
20
21
22
23
24
25
26
27
28
29
30
31
32
33
34
35
36
37
38
39
40
41
42
43
44
45
46
47
48
49
50
51
52
53
54
55
56
57
58
59
60
52. McLean, K. J., Warman, A. J., Seward, H. E., Marshall, K. R., Girvan, H. M., Cheesman, M. R., Waterman, M. R., and Munro, A. W. (2006) Biophysical characterization of the sterol demethylase P450 from *Mycobacterium tuberculosis*, its cognate ferredoxin, and their interactions, *Biochemistry* *45*, 8427-8443.
 53. Sun, Y. H., Zeng, W. Q., Benabbas, A., Ye, X., Denisov, I., Sligar, S. G., Du, J., Dawson, J. H., and Champion, P. M. (2013) Investigations of heme ligation and ligand switching in cytochromes P450 and P420, *Biochemistry* *52*, 5941-5951.
 54. Dawson, J. H., Andersson, L. A., and Sono, M. (1982) Spectroscopic investigations of ferric cytochrome P-450cam ligand complexes - Identification of the ligand trans to cysteine in the native enzyme, *J. Biol. Chem.* *257*, 3606-3617.
 55. Hyde, J. S., Rist, G. H., and Eriksson, L. E. (1968) ENDOR of methyl matrix and alpha protons of amorphous and polycrystalline matrices, *J. Phys. Chem.* *72*, 4269-&.
 56. Lobrutto, R., Scholes, C. P., Wagner, G. C., Gunsalus, I. C., and Debrunner, P. G. (1980) Electron nuclear double resonance of iron III cytochrome P450cam, *J. Am. Chem. Soc.* *102*, 1167-1170.
 57. Davydov, R., Dawson, J. H., Perera, R., and Hoffman, B. M. (2013) The use of deuterated camphor as a substrate in H-1 ENDOR studies of hydroxylation by cryoreduced oxy P450cam provides new evidence of the involvement of compound I, *Biochemistry* *52*, 667-671.
 58. Scholes, C. P., Feher, G., and Isaacson, R. A. (1972) Electron neutron double-resonance studies on heme proteins - Determination of interaction of Fe³⁺ with its ligand nitrogens in metmyoglobin, *Biochim. Biophys. Acta.* *263*, 448-&.
 59. Fann, Y. C., Gerber, N. C., Osmulski, P. A., Hager, L. P., Sligar, S. G., and Hoffman, B. M. (1994) ENDOR determination of heme ligation in chloroperoxidase and comparison with cytochrome P-450cam *J. Am. Chem. Soc.* *116*, 5989-5990.
 60. Davydov, R., Makris, T. M., Kofman, V., Werst, D. E., Sligar, S. G., and Hoffman, B. M. (2001) Hydroxylation of camphor by-reduced oxy-cytochrome P450cam: Mechanistic implications of EPR and ENDOR studies of catalytic intermediates in native and mutant enzymes, *J. Am. Chem. Soc.* *123*, 1403-1415.
 61. Scholes, C. P., Falkowski, K. M., Chen, S., and Bank, J. (1986) Electron nuclear double-resonance (ENDOR) of bis(imidazole)-ligated low-spin ferric heme systems, *J. Am. Chem. Soc.* *108*, 1660-1671.
 62. Uno, T., Nishimura, Y., Makino, R., Iizuka, T., Ishimura, Y., and Tsuboi, M. (1985) The Resonance Raman frequencies of the Fe-CO stretching and bending modes in the CO complex of cytochrome P450 cam, *J. Biol. Chem.* *260*, 2023-2026.
 63. Mak, P. J., Denisov, I. G., Grinkova, Y. V., Sligar, S. G., and Kincaid, J. R. (2011) Defining CYP3A4 structural responses to substrate binding. Raman spectroscopic studies of a nanodisc-incorporated mammalian cytochrome P450, *J. Am. Chem. Soc.* *133*, 1357-1366.
 64. Spiro, T. G., Soldatova, A. V., and Balakrishnan, G. (2013) CO, NO and O-2 as vibrational probes of heme protein interactions, *Coord. Chem. Rev.* *257*, 511-527.
 65. Collman, J. P., Sorrell, T. N., Dawson, J. H., Trudell, J. R., Bunnenberg, E., and Djerassi, C. (1976) Magnetic circular dichroism of ferrous carbonyl adducts of cytochromes P450 and P420 and their synthetic models - Further evidence for mercaptide as 5th ligand to iron, *Proc. Natl. Acad. Sci. U. S. A.* *73*, 6-10.

- 1
2
3
4
5
6
7
8
9
10
11
12
13
14
15
16
17
18
19
20
21
22
23
24
25
26
27
28
29
30
31
32
33
34
35
36
37
38
39
40
41
42
43
44
45
46
47
48
49
50
51
52
53
54
55
56
57
58
59
60
66. Wells, A. V., Li, P. S., Champion, P. M., Martinis, S. A., and Sligar, S. G. (1992) Resonance Raman investigations of Escherichia coli expressed Pseudomonas putida cytochrome P450 and P420, *Biochemistry* 31, 4384-4393.
67. Sabat, J., Stuehr, D. J., Yeh, S. R., and Rousseau, D. L. (2009) Characterization of the proximal ligand in the P420 form of inducible nitric oxide synthase, *J. Am. Chem. Soc.* 131, 12186-12192.
68. Cheesman, M. R., Zumft, W. G., and Thomson, A. J. (1998) The MCD and EPR of the heme centers of nitric oxide reductase from Pseudomonas stutzeri: Evidence that the enzyme is structurally related to the heme-copper oxidases, *Biochemistry* 37, 3994-4000.
69. Dhawan, I. K., Shelver, D., Thorsteinsson, M. V., Roberts, G. P., and Johnson, M. K. (1999) Probing the heme axial ligation in the CO-sensing CooA protein with magnetic circular dichroism spectroscopy, *Biochemistry* 38, 12805-12813.
70. McKnight, J., Cheesman, M. R., Thomson, A. J., Miles, J. S., and Munro, A. W. (1993) Identification of charge-transfer transitions in the optical spectrum of low-spin ferric cytochrome P-450 Bacillus megaterium, *Eur. J. Biochem.* 213, 683-687.
71. Gadsby, P. M. A., and Thomson, A. J. (1990) Assignment of the axial ligands of ferric ion in low-spin hemoproteins by near-infrared magnetic circular dichroism and electron paramagnetic resonance spectroscopy, *J. Am. Chem. Soc.* 112, 5003-5011.
72. Sono, M., Dawson, J. H., and Hager, L. P. (1984) The generation of a hyperporphyrin spectrum upon thiol binding to ferric chloroperoxidase - Further evidence of endogenous thiolate ligation to the ferric enzyme, *J. Biol. Chem.* 259, 3209-3216.
73. Bradley, J. M., Marritt, S. J., Kihlken, M. A., Haynes, K., Hemmings, A. M., Berks, B. C., Cheesman, M. R., and Butt, J. N. (2012) Redox and chemical activities of the hemes in the sulfur oxidation pathway enzyme SoxAX, *J. Biol. Chem.* 287, 40350-40359.
74. Nguyen, T. A., Jo, M. H., Choi, Y. G., Park, J., Kwon, S. C., Hohng, S., Kim, V. N., and Woo, J. S. (2015) Functional Anatomy of the Human Microprocessor, *Cell* 161, 1374-1387.
75. Kwon, S. C., Nguyen, T. A., Choi, Y. G., Jo, M. H., Hohng, S., Kim, V. N., and Woo, J. S. (2016) Structure of Human DROSHA, *Cell* 164, 81-90.
76. Driscoll, M. D., McLean, K. J., Levy, C., Mast, N., Pikuleva, I. A., Lafite, P., Rigby, S. E. J., Leys, D., and Munro, A. W. (2010) Structural and Biochemical Characterization of Mycobacterium tuberculosis CYP142, *J. Biol. Chem.* 285, 38270-38282.
77. Daff, S. N., Chapman, S. K., Turner, K. L., Holt, R. A., Govindaraj, S., Poulos, T. L., and Munro, A. W. (1997) Redox control of the catalytic cycle of flavocytochrome P-450 BM3, *Biochemistry* 36, 13816-13823.
78. Spiro, T. G., and Wasbotten, I. H. (2005) CO as a vibrational probe of heme protein active sites, *J Inorg Biochem* 99, 34-44.

FIGURE LEGENDS

Figure 1. UV-vis absorption properties of the human $\Delta 276$ DGCR8 protein. Panel A shows oxidized DGCR8 (4.1 μM , red line) with split Soret features and maxima at 450 nm and 367 nm. There is a broad, low intensity feature in the Q-band region stretching from ~ 530 -630 nm. On reduction of the sample with sodium dithionite, a single Soret feature is seen at 427 nm, with asymmetric bands in the visible region at 531 and 559 nm (green line). The binding of carbon monoxide to the reduced DGCR8 protein produces the Fe^{II} -CO complex with its Soret maximum at 421 nm and a partial merging of visible bands to give peaks at approximately 540 nm and 570 nm (blue line). **Panel B** shows a partially reduced DGCR8 sample (6 μM , black line), with a Soret maximum at 427 nm and visible region bands at 529 and 559 nm. The binding of O_2 results in a 5 nm shift to a Soret maximum of 422 nm with merging of the visible bands (peak at 557 nm, red line). The ferrous-oxy DGCR8 rapidly collapses back to the ferric form, and a shoulder at 450 nm is apparent in the spectrum for the O_2 -bound form, consistent with a mixture of ferric and ferrous-oxy species. The ferrous-oxy UV-vis spectrum was collected by stopped-flow spectroscopy 25 ms after mixing the reduced sample with O_2 -saturated buffer.

Figure 2. EPR and ENDOR spectroscopy of DGCR8. **Panel A.** X-band continuous wave EPR spectrum of human DGCR8 recorded at 10 K with g -values marked. **Panel B.** X-band Davies pulsed ENDOR spectra of human DGCR8 obtained at 10 K showing the region around the ^1H Larmor frequency; a resolved hyperfine coupling of 5.1 MHz is marked together with the largest exchangeable proton hyperfine coupling of 2.4 MHz. **Panel C.** X-band Davies pulsed ENDOR spectrum of human DGCR8 obtained at 10 K showing the low frequency region; analysis indicating a single ^{14}N hyperfine coupling and quadrupole splitting is shown.

1
2
3 **Figure 3. Resonance Raman spectroscopy of DGCR8. Panel A.** The high-frequency RR
4 spectrum for the ferric DGCR8 acquired with a 441.6 nm laser line. (85 μM ferric DGCR8, in 50
5 mM Tris pH 8.0, containing 500 mM KCl and 10% glycerol). The inset shows the region from
6 $\sim 1390\text{ cm}^{-1}$ upwards for the ferric DGCR8 in 10% glycerol buffer (a), ferric DGCR8 in the same
7 buffer without glycerol (b), and their difference trace (c). **Panel B.** The high-frequency RR
8 spectrum for the ferrous DGCR8 acquired with a 415 nm laser line (85 μM DGCR8 reduced
9 under an inert atmosphere of N_2 with a 20-fold molar excess of sodium dithionite in the presence
10 of methyl viologen and benzyl viologen). **Panel C.** The low-frequency (left-side of each
11 spectrum) and high-frequency (right-side of each spectrum) RR spectral region of the ferrous-CO
12 adducts of DGCR8. The upper traces show the RR spectrum for the $\text{Fe}^{\text{II}}\text{-}^{12}\text{CO}$ adduct, whereas
13 the lower traces show the $\text{Fe}^{\text{II}}\text{-}^{13}\text{CO}$ adduct. The traces in the central panels show the ^{12}CO minus
14 ^{13}CO difference plots in the $\nu_{(\text{Fe-C})}$ and $\nu_{(\text{C-O})}$ regions, respectively. **Panel D.** The CO-
15 backbonding correlation lines of P450cam (L = thiolate), histidine ligated enzymes (L = His) and
16 NOS (L = thiolate) (78). Data points (\bullet) are associated with a heme-thiol model complex,
17 DGCR8 (this study), and iNOS P420 and iNOS P450 forms (67).
18
19
20
21
22
23
24
25
26
27
28
29
30
31
32
33
34
35
36
37
38
39
40
41
42
43
44

45 **Figure 4. UV-vis and near-infrared MCD spectra for DGCR8. Panel A** shows the UV-vis
46 MCD spectrum for ferric DGCR8 (70 μM), with a derivative at 451 nm and a strong negative
47 feature at 600 nm. **Panel B** shows the near-infrared MCD spectrum for ferric DGCR8 (70 μM)
48 with a strong band at 1260 nm reporting on the coordination state of the heme iron. **Panel C**
49 shows the UV-vis MCD spectrum for the ferrous form of DGCR8 (185 μM), with a feature at
50 436 nm and a derivative at 556 nm.
51
52
53
54
55
56
57
58
59
60

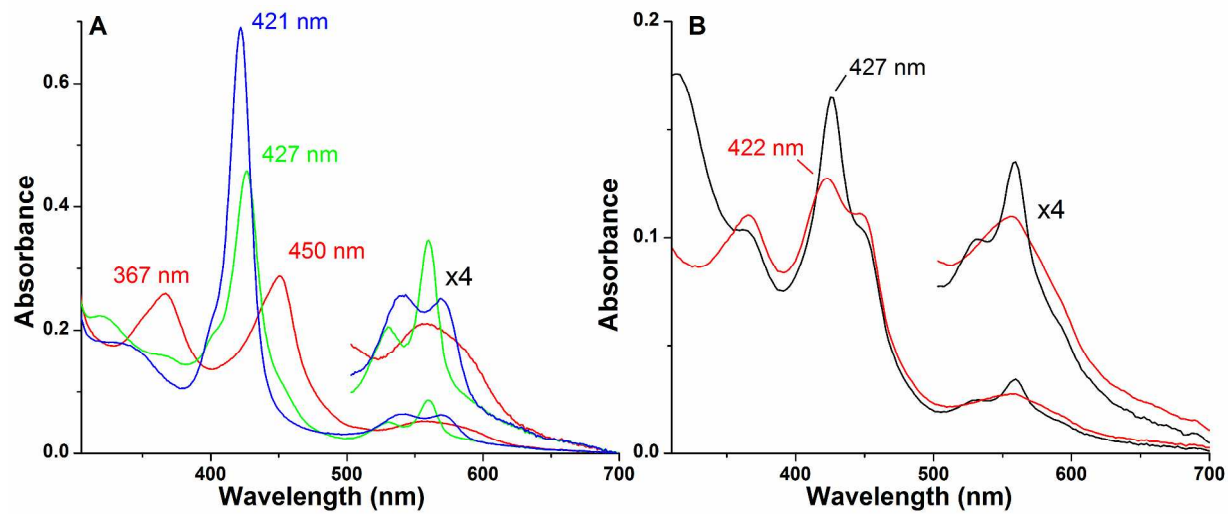


Figure 1

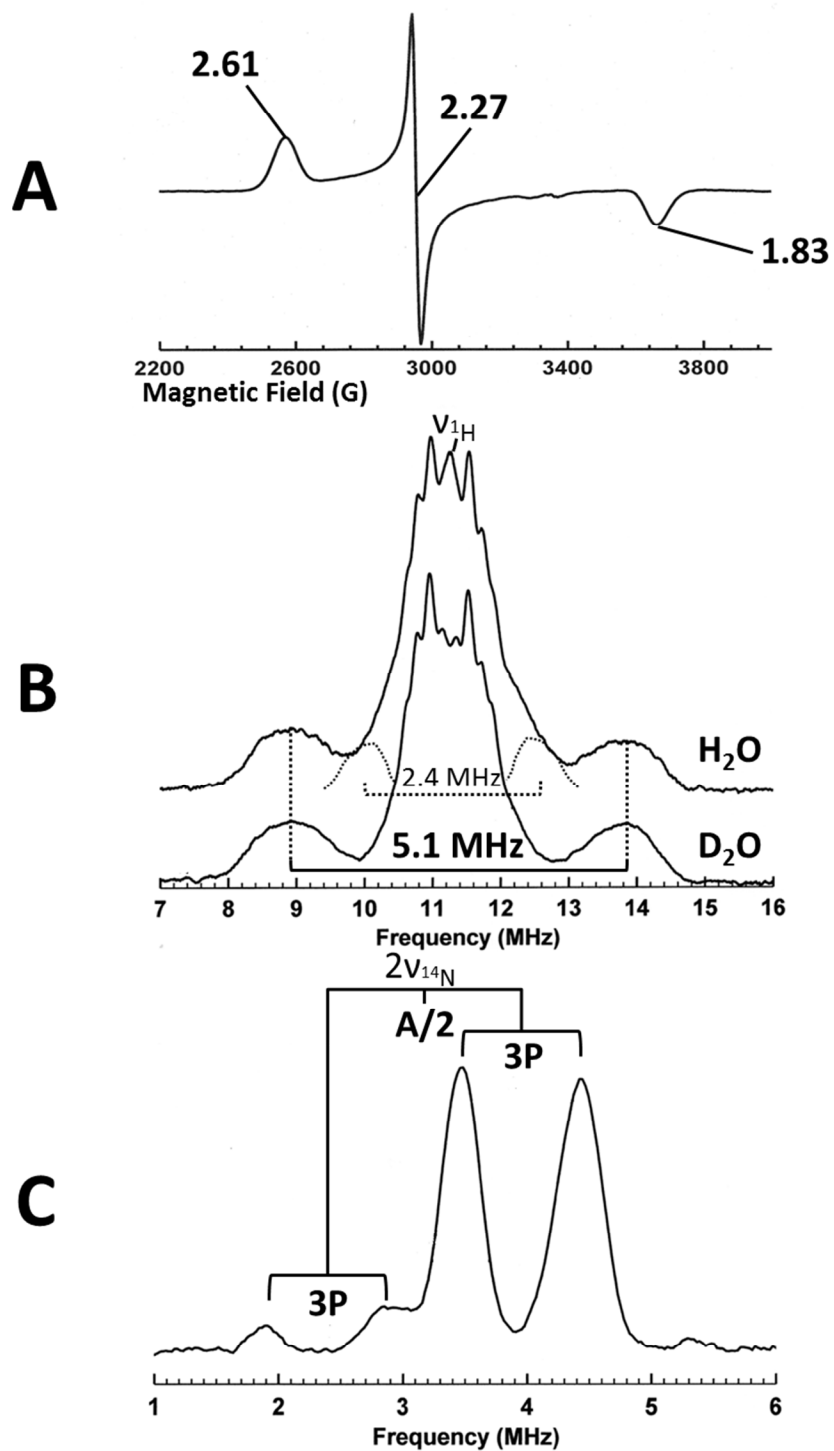


Figure 2

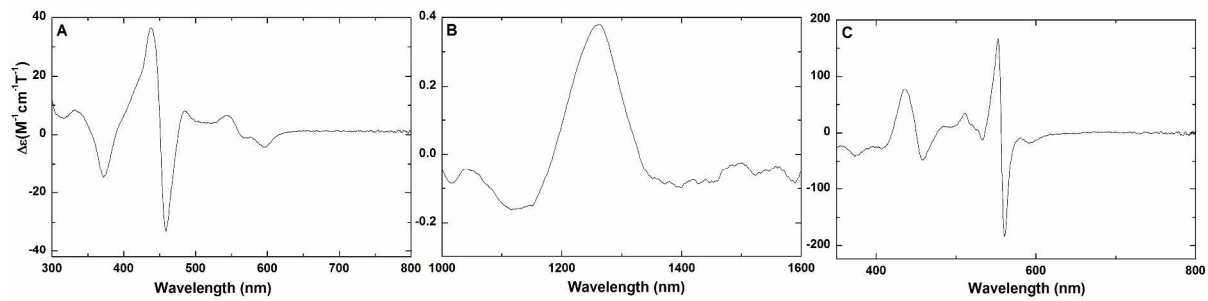
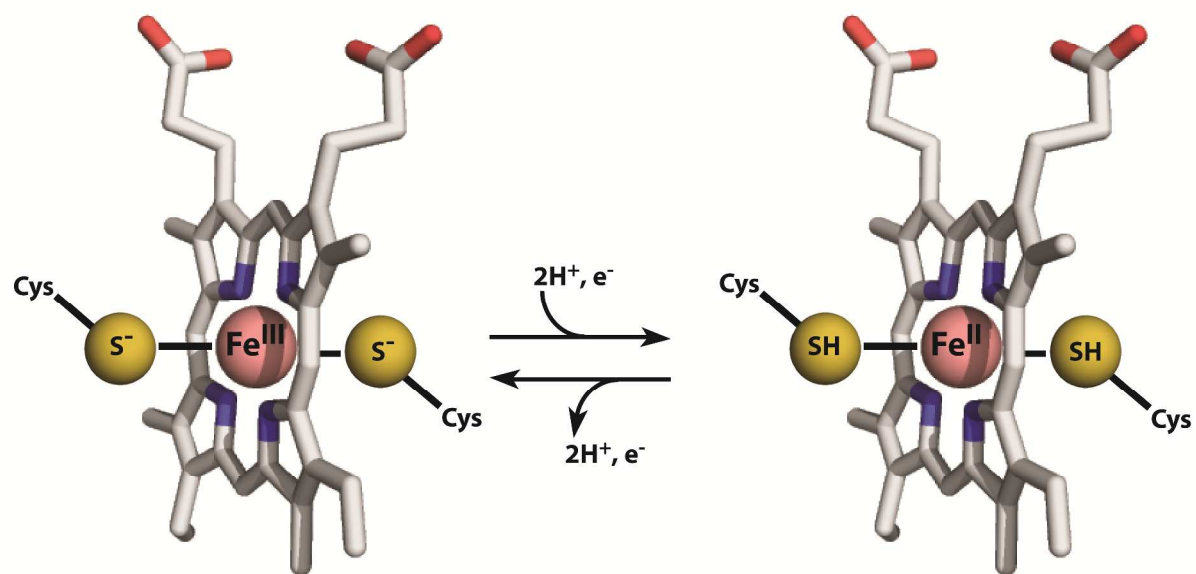


Figure 4

Graphic for Table of Contents



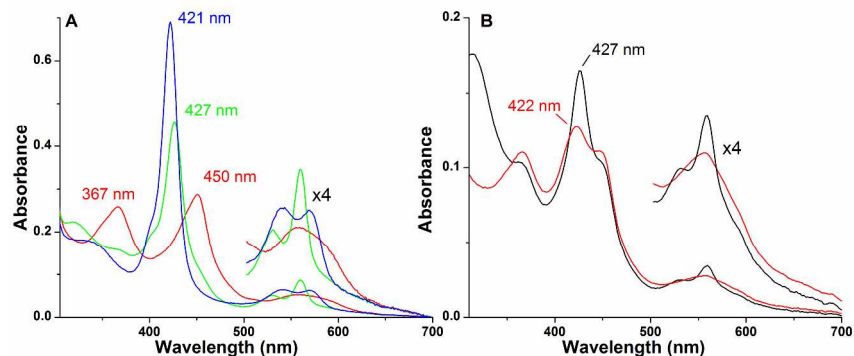


Figure 1. UV-vis absorption properties of the human $\Delta 276$ DGCR8 protein. Panel A shows oxidized DGCR8 (4.1 μM , red line) with split Soret features and maxima at 450 nm and 367 nm. There is a broad, low intensity feature in the Q-band region stretching from ~ 530 -630 nm. On reduction of the sample with sodium dithionite, a single Soret feature is seen at 427 nm, with asymmetric bands in the visible region at 531 and 559 nm (green line). The binding of carbon monoxide to the reduced DGCR8 protein produces the $\text{Fe}^{\text{II}}\text{-CO}$ complex with its Soret maximum at 421 nm and a partial merging of visible bands to give peaks at approximately 540 nm and 570 nm (blue line). Panel B shows a partially reduced DGCR8 sample (6 μM , black line), with a Soret maximum at 427 nm and visible region bands at 529 and 559 nm. The binding of O_2 results in a 5 nm shift to a Soret maximum of 422 nm with merging of the visible bands (peak at 557 nm, red line). The ferrous-oxy DGCR8 rapidly collapses back to the ferric form, and a shoulder at 450 nm is apparent in the spectrum for the O_2 -bound form, consistent with a mixture of ferric and ferrous-oxy species. The ferrous-oxy UV-vis spectrum was collected by stopped-flow spectroscopy 25 ms after mixing the reduced sample with O_2 -saturated buffer.

1
2
3
4
5
6
7
8
9
10
11
12
13
14
15
16
17
18
19
20
21
22
23
24
25
26
27
28
29
30
31
32
33
34
35
36
37
38
39
40
41
42
43
44
45
46
47
48
49
50
51
52
53
54
55
56
57
58
59
60

Figure 1
367x520mm (300 x 300 DPI)

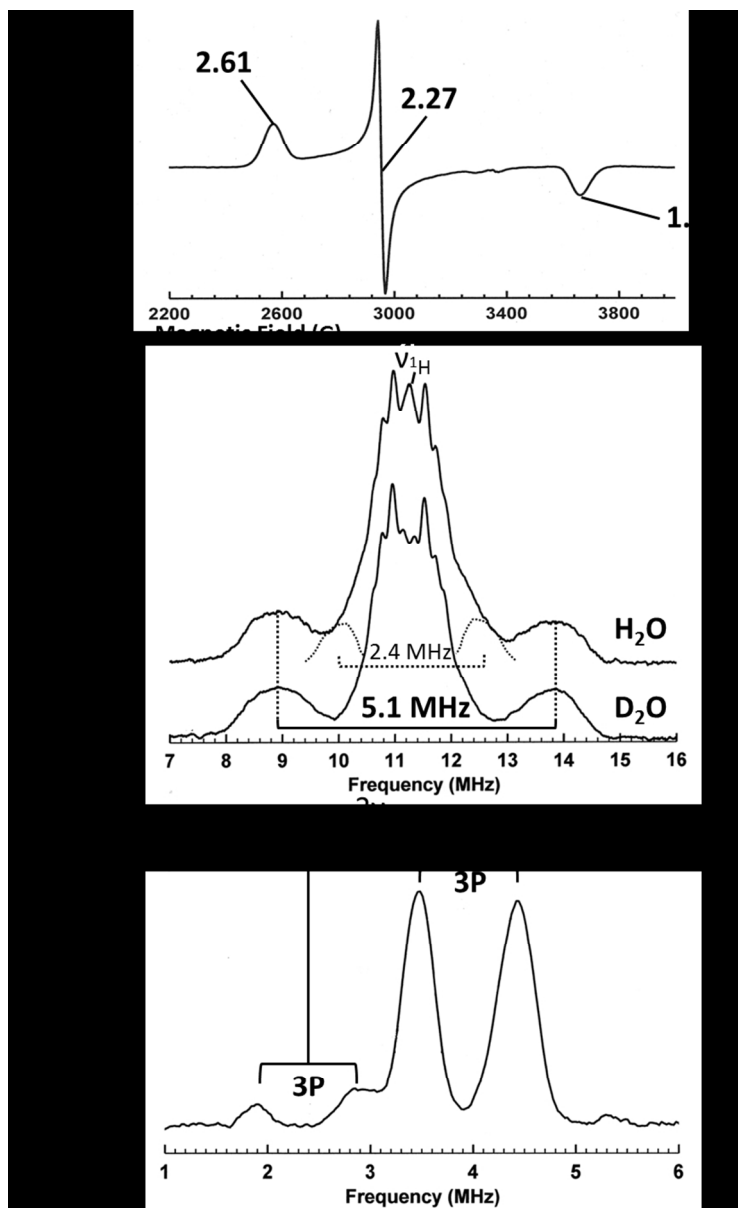


Figure 2. EPR and ENDOR spectroscopy of DGCR8. Panel A. X-band continuous wave EPR spectrum of human DGCR8 recorded at 10 K with g -values marked. Panel B. X-band Davies pulsed ENDOR spectra of human DGCR8 obtained at 10 K showing the region around the ^1H Larmor frequency; a resolved hyperfine coupling of 5.1 MHz is marked together with the largest exchangeable proton hyperfine coupling of 2.4 MHz. Panel C. X-band Davies pulsed ENDOR spectrum of human DGCR8 obtained at 10 K showing the low frequency region; analysis indicating a single ^{14}N hyperfine coupling and quadrupole splitting is shown.

Figure 2

147x239mm (150 x 150 DPI)

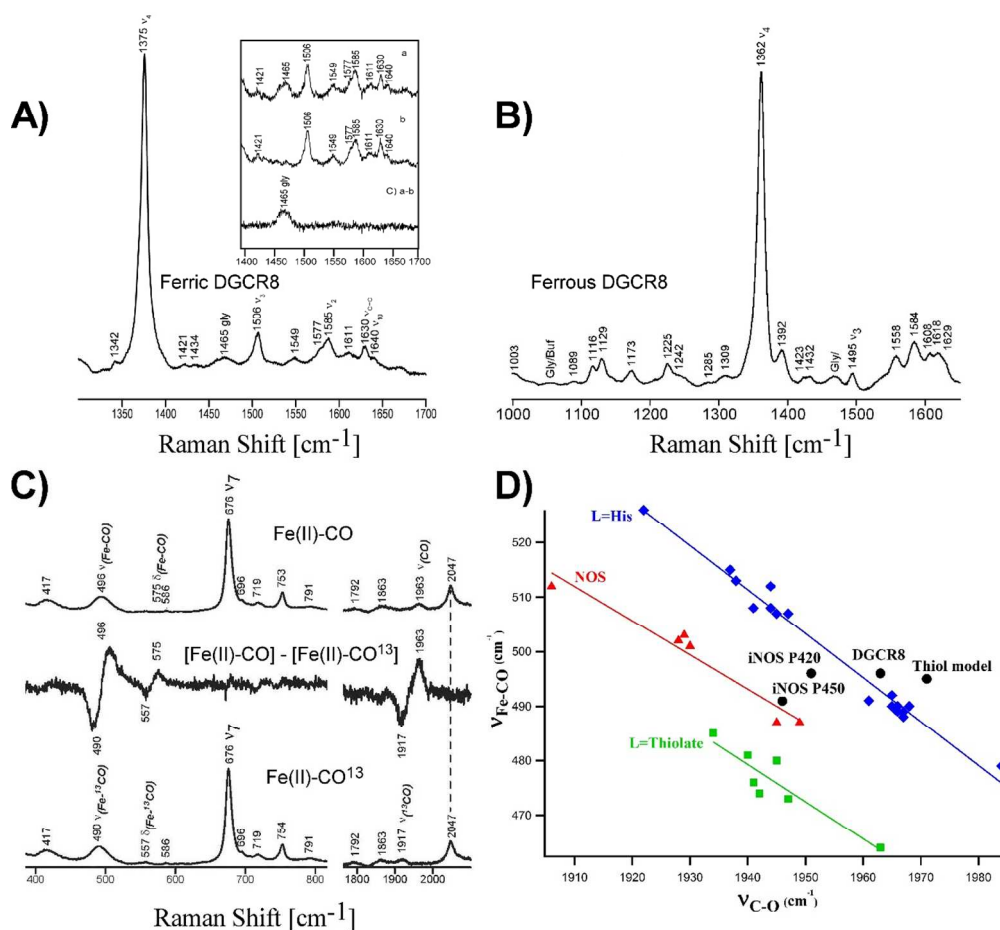


Figure 3. Resonance Raman spectroscopy of DGCR8. Panel A. The high-frequency RR spectrum for the ferric DGCR8 acquired with a 441.6 nm laser line. (85 μ M ferric DGCR8, in 50 mM Tris pH 8.0, containing 500 mM KCl and 10% glycerol). The inset shows the region from \sim 1390 cm^{-1} upwards for the ferric DGCR8 in 10% glycerol buffer (a), ferric DGCR8 in the same buffer without glycerol (b), and their difference trace (c). Panel B. The high-frequency RR spectrum for the ferrous DGCR8 acquired with a 415 nm laser line (85 μ M DGCR8 reduced under an inert atmosphere of N_2 with a 20-fold molar excess of sodium dithionite in the presence of methyl viologen and benzyl viologen). Panel C. The low-frequency (left-side of each spectrum) and high-frequency (right-side of each spectrum) RR spectral region of the ferrous-CO adducts of DGCR8. The upper traces show the RR spectrum for the $\text{Fe}^{\text{II}}_{12}\text{CO}$ adduct, whereas the lower traces show the $\text{Fe}^{\text{II}}_{13}\text{CO}$ adduct.

The traces in the central panels show the ^{12}CO minus ^{13}CO difference plots in the $\nu(\text{Fe}-\text{C})$ and $\nu(\text{C}-\text{O})$ regions, respectively. Panel D. The CO-backbonding correlation lines of P450cam (L = thiolate), histidine ligated enzymes (L = His) and NOS (L = thiolate) (76). Data points (\bullet) are associated with a heme-thiol model complex, DGCR8 (this study), and iNOS P420 and iNOS P450 forms (67).

159x146mm (220 x 220 DPI)

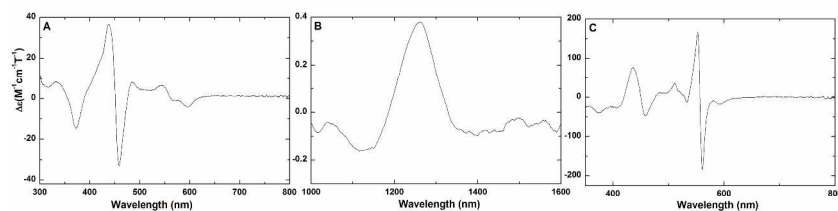


Figure 4. UV-visible and near-infrared MCD spectra for DGCR8. Panel A shows the UV-vis MCD spectrum for ferric DGCR8 (70 μM) with a derivative at 451 nm and a strong negative feature at 600 nm. Panel B shows the near-infrared MCD spectrum for ferric DGCR8 (70 μM) with a strong band at 1260 nm reporting on the coordination state of the heme iron. Panel C shows the UV-vis MCD spectrum for the ferrous form of DGCR8 (185 μM), with a feature at 436 nm and a derivative at 556 nm.

389x557mm (300 x 300 DPI)